# Degradation of Rhodamine B using Cu-Doped $SrFeO_3$ thermocatalysts

Master Thesis

Andreas Kruse Pedersen

Aalborg Universitet
Chemistry

**Chemistry and Bioscience**
Aalborg University
http://www.aau.dk

**AALBORG UNIVERSITY**
STUDENT REPORT

**Title:**
Degradation of Rhodamine B using Cu-Doped $SrFeO_3$ thermocatalysts

**Theme:**
Master thesis

**Project Period:**
September 1, 2023 - June 3, 2024

**Participant(s):**
Andreas Kruse Pedersen

**Supervisor(s):**
Martin Bonderup Østergaard

**Copies:** 1

**Page Numbers:** 51

**Date of Completion:**
June 3, 2024

**Abstract:**

The perovskite oxide, Strontium ferrate ($SrFeO_3$), was synthesized through solution combustion synthesis with a copper concentration varying between 0-10%. This was done to investigate the effect of B-site on $Fe^{4+}$-ions generation for the degradation of rhodamine B through thermal catalysis under dark ambient conditions. XPS results showed that with the increase in copper content, the proportion of $Fe^{4+}$-ions would increase as well as the amount of oxygen present in the lattice of the perovskites compared to the surface. UV-Vis measurement showed full degradation of rhodamine B when not recycling the perovskite. The activation energy decreased showing a minimum at 5% copper Doping. The perovskites were able to degrade rhodamine B fully however, When the perovskite is recycled a hypsochromic shift is seen. This shift was assumed to be the *N*-deethylization of rhodamine B into rhodamine 110 causing the liquid to turn green. During recycling the rate of degradation decreased after each cycle which could be caused by the leaching of metals. AAS results showed an extensive leaching of all metals into the solution during thermal catalysis. This could be an indication that the stability of the perovskite is low. In general $SrFeO_3$ can degrade rhodamine B however the perovskite is quickly weakened by extensive leaching and struggles to degrade after multiple recycles. For future work, it could be interesting to try and minimize the leaching by potentially exploring other dopants. It could also be interesting to degrade other organic pollutants to see how the perovskite evolves/devolves when recycled.

# List of abbreviations

- **Abbreviation - Meaning**
- F/M - Fuel to metal cation ratio
- SCS - Solution combustion synthesis
- XRD - X-ray diffraction
- FT-IR - Fourier-transform infrared spectroscopy
- GoF = Goodness of fit test
- Rh-B = Rhodamine B
- Rh-110 = Rhodamine 110
- AOP = Advanced Oxidation Processes
- ROS = Reactive Oxygen Species
- AAS = Atomic absorption spectroscopy
- $SrFeO_3$ = Strontium ferrate

# Contents

# Preface

This project was performed between September 1, 2023 and June 3, 2024, by Andreas Kruse Pedersen at Aalborg University. The project supervisor was Martin Bonderup Østergaard.

Aalborg University, June 3, 2024

Andreas Kruse Pedersen
akpe19@student.aau.dk
Study number: 20194730

# Chapter 1
# Introduction

With a growing population worldwide, an increased consumption of organic compounds occurs causing pollution. The pollutants that result from these are called emerging organic contaminants (EOCs). EOCs usually come from pharmaceuticals, industrial chemicals, pesticides, surfactants, food additives, and more [1]. To make sure that EOCs remain harmless PNEC-values (Predicted no effect concentration) were implemented indicating the harmful limit of a specific contaminant [2]. Pollution source control exists, but apart from that different approaches to minimize organic pollutants are in use. These approaches can be characterized into 3 groups, which are, physical methods, biological treatment, and chemical treatment.

The physical method is the treatment of organic pollutants using methods such as adsorption, flocculation, sedimentation, filtration, etc. Physical methods are generally free of chemical or biological interventions and instead use naturally occurring forces to remove substances. These forces include gravity, electrical attraction, and van der Waals forces. To generalize, no change in the chemical structure of the substance. The physical state of the substance may be changed in some cases if vaporized or dispersed substances agglomerate during filtration [3]. The downside to the physical method is if you use treatments such as adsorption with activated carbon it loses between 10-15% of the sorbent which results in the need for regeneration.

biological treatment uses microorganisms or enzymes to break down high-molecular-weight compounds into smaller and simpler molecules through biodegradation. A downside to biological treatments are very sensitive because organisms are not fully effective, causing poor applicability [3].

The chemical method is when biological and physical treatment falter. The chemical method is a treatment where the contaminants are either removed or converted into less- or non-harmful materials. This is done with the addition of chemicals that target the desired contaminants to be removed by chemical reactions. Examples of chemical methods are precipitation, adsorption, and disinfection. Additional chemicals are also used to enhance the process. A problem with the use of additional chemicals is that they can end up as secondary pollution. Due to this problem another chemical cleaning method, known as advanced oxidation processes (AOPs), is becoming a more common technique. AOPs utilize highly reactive species called reactive oxygen species (ROS). Some of the possible generated ROS are $OH^{\bullet}$, $O_2^{\bullet -}$, $HO_2^{\bullet -}$ and $SO_2^{\bullet -}$ which can mineralize the pollutant into non-toxic/less toxic products such as $H_2O$, $CO_2$, and salts [1, 3].

The dye industry emits many polluting dyes such as methyl orange, eosin Y, methyl blue, rhodamine B (Rh-B), etc. [4]. The organic pollutant analyzed throughout this report is a chemical dye called Rh-B (**Figure 1.1**). Rh-B is usually used for industrial purposes such as printing and dying of textiles, paints, paper, etc [5]. Rh-B is said to cause skin and eye irritation and can be

harmful if swallowed irritating the respiratory tract [6].

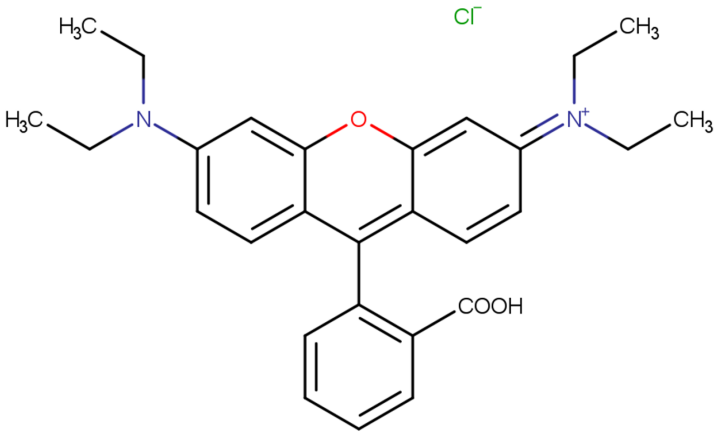


**Figure 1.1:** Structure of Rh-B

Thermal catalysis is a promising AOP and has advantages compared to other AOPs such as photocatalysis. For organic polluted wastewater treatment, thermal catalysis can reach far more problematic places compared to other AOPs. An example is photocatalysis which is limited in places without sunlight such as underground cleaning systems. Thermal catalysis is also operational in soil whereas other AOPs are limited. Examples of materials used in thermal catalysis under dark ambient conditions are single metal oxide/salts, hydrates, and perovskites [1].

The original perovskite had the crystal structure of $CaTiO_3$, however, it was discovered that the perovskite structure was not limited to this specific mineral. Perovskite would later get the general formula of $ABX_3$ representing a combination of different organic and inorganic ions [7]. Perovskites are in general one of the most abundant crystal structures on the planet and are therefore easily accessible making it a cheap and cost-efficient material [8].
A great feature of perovskite is their ease of modification in the sense that the A-/B-sites can be replaced by 90% of the periodic table [1]. This gives great interest to the perovskites to enhance their properties such as chemical stability and prevent the possibility of leaching. Increasing the catalytic effect is also possible through doping. A promising perovskite used for the degradation of organic pollutants is Strontium ferrate ($SrFeO_3$). A common A-site dopant of $SrFeO_3$ that is analyzed in the literature is cerium [9, 10, 11]. An example of A and B site doping is Dou et al. who codoped $SrFeO_3$ with cobalt and calcium. Calcium would substitute strontium whereas cobalt would substitute iron [12]. An interesting aspect of $SrFeO_3$ is the potential increase of its catalytic effect through B-site doping. This would occur if the dopant has a charge of +2 or lower which would in theory create more $Fe^{4+}$-ions and possibly increase the catalytic effect of the perovskite. Throughout this report, $SrFeO_3$ doped with copper, zinc, or nickel separately is analyzed because their most abundant iron has a charge of +2.

# Chapter 2
# Problem Statement

Thermal catalysis under dark ambient conditions can be categorized as an AOP with advantages such as energy and chemical consumption compared to other AOP.
Possible materials used for thermal catalysis are perovskites. Perovskite can be modified in many different ways to enhance its properties such as stability and catalytic effect. The doping of B-site for catalytic perovskites is limited in literature and is, therefore, the focus of this project where the perovskite $SrFeO_3$ will be doped with either copper, zinc, or nickel. This is to investigate how the doping of b-sites affects the $Fe^{4+}$-ion content in the perovskite and leads to the following problem statement:

## How does the doping of strontium ferrate affect its ability to degrade Rhodamine B?

The problem statement will be addressed and understood through the following sub-goals:

- Synthesis of doped $SrFeO_3$ ranging from 0-10% Copper, nickel and zinc
- Perovskite characterization by XRD to confirm single phase structure.
- Measuring full spectrum UV-vis spectroscopy during the thermal catalytic experiment to analyze how the doping affects the degradation of Rh-B.
- Analyzing the possibility of leaching through Atomic absorption spectroscopy (AAS) to indicate the stability of the perovskites.
- Analyzing the surface chemistry through XPS to determine iron ion content and oxygen vacancies.

# Chapter 3
# Theory

## 3.1 Perovskite

Inorganic/organic perovskites have a general formula of $ABX_3$ where A is a large cation, usually alkali metals or alkaline earth metals. B is a medium/small transition metal cation and X represents an anion (O if it is categorized as a perovskite oxide) [13].
For perovskites with the structure of $ABX_3$ the A-site cation is a 12-coordinated metal, while the B-site cation is coordinated with six oxygen-atoms as corner-sharing $BO_6$ octahedrons [13, 14]. The stability and physical properties of perovskite oxides are dependent on the B-site metal ion. Wang et al. explains that for a perovskite to be stable the B-site cations should be larger than 0.51 Å. The A-site cations size affects the symmetry of the perovskite oxide meaning the size of both A- and B-site cations should be considered to create the preferred cubic structure [13]. Because of that a tolerance factor, $t$, which is based on an empirical equation, is implemented by Goldschmidt (**Equation 3.1**). The accuracy of the tolerance factor is limited due to it only accounting for the chemical formula and the ionic radii of each ion.

$$t = \frac{R_A + R_O}{\sqrt{2} \cdot (R_B + R_O)} (0.75 < t < 1.13) \tag{3.1}$$

Here $R_A$, $R_B$, and $R_O$ are the radii of A-, B- and O-site ions. For perovskite oxide, the most stable perovskite structure is a symmetric cubic structure. A general rule is that if the t-value is between 0.75 and 1.13 the perovskites structure is stable [13]. Having a t-value close to 1 a cubic structure is obtained called "aristotype" which represents the highest order of symmetry. If the t-value is within the interval of $0.9 < t < 0.8$ a tetragonal structure is obtained and if it's smaller than 0.8 an orthorhombic structure is obtained as shown in **Figure 3.1**.

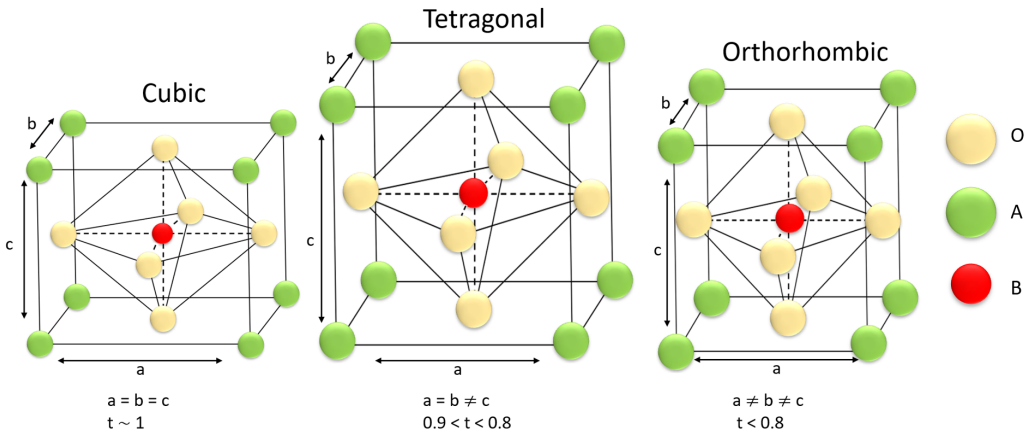


**Figure 3.1:** The figure shows different perovskite oxide structures of $ABO_3$ depending on t-value. Inspired by [15, 16].

As mentioned in **Chapter 1** perovskites can greatly be modified. This gives great interest to the perovskites to enhance their properties such as chemical stability and prevent the possibility of leaching. Increasing the catalytic effect is also possible through doping as it can possibly change the oxidation state of the perovskite.

Multiple perovskites have been used for the degradation of organic pollutants. Ismael and Wark observed undoped $LaFeO_3$ as promising photocatalyst degrading Rhodamine B and 4-chlorophenol [17]. Similarly Kappadan et al. tested undoped $BaTiO_3$ as a photocatalyst for the degradation of methylene blue. They saw, over 50 minutes, that the perovskite was capable of degrading 50% and 64% of the dye when 50 mg and 70 mg of the catalyst were used. However, when exceeding 70 mg the effectiveness of the catalyst would decrease[18]. Zhong et al. explored the degradation of methyl orange azo dye in aqueous solution under dark ambient conditions and observed a degradation percentage of 94.3% after undergoing 4 hours thermal catalysis [19]. These are just some examples of perovskites used for the degradation of organic pollutants, however, in this project, the focus will be on the perovskite $SrFeO_3$ due to strontium being a promising A-site cation and iron having an uncommon oxidation state of +4 which possibly enhances its catalytic abilities [11, 14].

### 3.1.1 Strontium ferrate

$SrFeO_3$ have the property of being able to accommodate a large range of oxygen deficiencies leading to the general formula of $SrFeO_{3-\delta}$ where $\delta$ is the oxygen non-stoichiometry value indicating the amount of oxygen vacancies present in the perovskite. Due to being able to accommodate oxygen deficiencies, $SrFeO_3$ creates $Fe^{3+}$-ions (which have a larger ionic radius), balancing the global neutral valance state. This results in a redox couple of $Fe^{4+}/Fe^{3+}$ [14]. according to Tummino, $SrFeO_3$ is cubic at $\delta = 0$, tetragonal at $\delta = 0.125$, orthorombic at $\delta = 0.25$ and brownmillerite-type at $\delta = 0.5$. If $\delta$ is between these numbers a mixed state will occur [14]. Wang et al. explains that the $\delta$-value is usually lower than 0.5. If it exceeds $\delta$ = 0.5, the amount of oxygen vacancies responds to around 17% which would cause the perovskite structure to collapse [13].

$SrFeO_3$ makes an interesting catalyst due to its ability to create oxygen vacancies from the redox couple. A schematic of oxygen vacancies in a perovskite is illustrated in **Figure 3.2**.

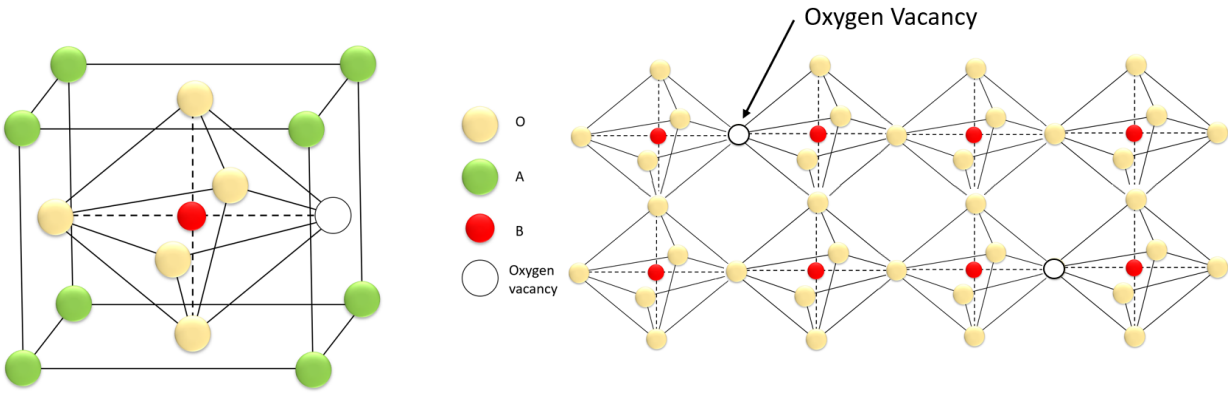


**Figure 3.2:** The figure shows a general perovskite structure with oxygen vacancies

Hwang et al. Indicates that the main catalytic sites are in the B-site, whereas according to Li et al. the A-site would control the band gap of the perovskite [20, 21]. $SrFeO_3$ is a stable perovskite

of cubic structure based on a t-value of 1.01. The values to calculate the t-value are based on Grimes database and calculations are based on **Equation 3.1**.
The ionic radius of strontium is 1.44 due to it being a 12-coordinated atom in the $SrFeO_3$ structure. Iron has an ionic radius of 0.585 as its oxidation state is +4. The charge of iron is based on Tummino which earlier stated that the majority of iron in $SrFeO_3$ is +4 charged. In $SrFeO_3$, oxygen is a six-coordinated atom and therefore has an ionic radius of 1.4 [22].

A downside to $SrFeO_3$ when used as a catalyst is the possible formation of carbonates. This can result in the blockage of the catalytic sites thereby decreasing its effectiveness. Deganello et al. found carbonate formation on freshly synthesized $Sr_{1-a}Ce_aFeO_{3-x}$ up to 30% after one month's exposure to air able to react with the $CO_2$ in the atmosphere [23]. This however is not in agreement with [9] who found no carbonate formation when only exposed to air for 195 days. A worthy notice is that the two studies use different methods of carbonate detection, X-ray photoelectron spectroscopy (XPS) and Fourier-transform infrared spectroscopy (FT-IR). XPS is far more sensitive in the outermost layer of the perovskites which is a possible explanation for the differences in the studies. It is therefore unclear what provokes this carbonate formation when exposed to air due to the inconsistencies. When the perovskite is exposed to water or used in a thermal catalytic sense Østergaard et al. learned that carbonate formation would occur. The carbonation that mainly occurred was $SrCO_3$ [9].

### 3.1.2 Doping of Perovskite

As mentioned earlier in **Chapter 1**, doping of perovskites is an attractive ability to enhance its properties. The doping of respectively A- and B-site of the perovskites gives different properties.

**A-site doping** When doping the A-site the structure and stability of the perovskite may increase Deganello et al. found that doping $SrFeO_3$ with cerium improved structure and reduction properties. However, this highly depended on the amount of cerium doping which ranged between 0 and 15%. When below 6% a cubic structure was seen however, when the Ce doping exceeded that, a tetragonal structure was obtained [23]. As mentioned earlier in 3.1.1, doping of the A-site would alter a change in the band gap of the perovskite.

**B-site doping** Sun et al. doped $SrFeO_3$ with copper and found out that it increases the oxygen vacancy concentration in the perovskite [24, 25]. When doping $SrFeO_3$ the crystal structure changes with the $\delta$-value. This also means that the structure of the perovskite may change from cubic to tetragonal or other possible structures [24]. Doping $SrFeO_3$ with copper or other materials with an oxidation state of +2 would in theory increase the $Fe^{+4}$-ion content in the perovskite as charge balancing would occur. As mentioned earlier in **Section 3.1.1**, the B-site is the main catalytic site which means that B-site doping would be the main focus point when trying to optimize the catalytic performance of perovskites.

## 3.2 Solution combustion synthesis

Solution combustion synthesis (SCS) is a promising method of producing inorganic nanomaterials with high reactivity through a simple and time/energy-saving method. SCS is a great

way of synthesizing single-phase compounds which are normally unable to be synthesized by conventional methods. It consists of three main steps which are (1) the formation of the combustion mixture, (2) the formation of gel, and (3) the combustion of the gel. An important part of the last step is that the combustion of the gel should happen in a rapid single step to ensure that no undesired products are formed. When the gel is fully combusted, a powder remains which shows great properties such as high surface area, great phase purity, narrow particle size distribution, etc.
SCS depends on many different parameters and the most influential are, fuel type, reducer-to-oxidizer ratio, fuel-to-metal cation ratio, and the pH of the solution [26]. Below, in **Figure 3.3**, a general schematic of which steps the SCS goes through.

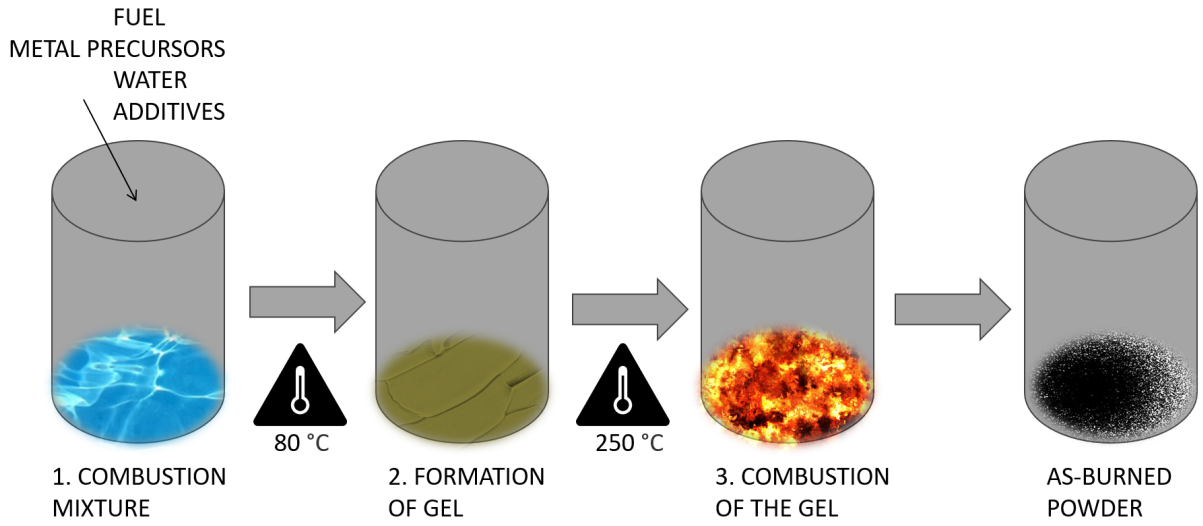


**Figure 3.3:** The figure illustrates the general steps associated with SCS. Inspired by [26]

.

### 3.2.1 Fuel type

Generally, a fuel is any organic compound that i capable of reacting with an oxidant to start a combustion process. In the SCS process, the fuel should be able to fulfill 4 objects. Firstly it should act as a reducer and be able to undergo an acceptable combustion with the oxidants at a relatively low ignition temperature. Secondly, it's preferred to be able to chelate metal cations in a gel. This results in the compositional homogeneity between the constituents being kept up. Thirdly it needs to be able to form a clear transparent gel when the water is evaporated. The fourth and last criterion of the fuel includes non-hygroscopic, economically reasonable, and easily obtainable [26]. If the fuel is hygroscopic it may lead to moisture from the atmosphere being included in the reaction altering the stoichiometry of the reaction mixture even though the solution is water-based. On top of these properties, the fuel will act as a microstructural template, resulting in different microstructures depending on the choice of fuel. A promising fuel for SCS is citric acid due to low heat of combustion resulting in the saving of time and energy.

### 3.2.2 Reducer to oxidizer ratio

The reducer to oxidizer ratio ($\phi$), also known as the fuel-to-oxidizer ratio and is expressed in the following equation:

$$\phi = \frac{(-1)RV}{OV}n \tag{3.2}$$

where RV is the reducer valence, OV is the oxidizer valence and n is the number of moles of fuel per mole of oxidizer. if $\phi > 1$ or $\phi < 1$ it is an indication of a fuel-rich or a fuel-poor solution. In a fuel-rich mixture impurities, such as carbon and carbonates, are more likely to occur because of the large amount of excess fuel [27].
When the stoichiometric combustion occurs (at $\phi = 1$) the right amount of oxygen and fuel mix is present. This causes the most heat possible and the efficiency of the combustion reaches its maximum [27].

### 3.2.3 Fuel to metal cation ratio

Fuel-to-metal cation ratio (F/M) is another important parameter when it comes to fuel selection and amount. It is however not straightforward when interpreting its role due to a low number of published studies. Nevertheless, it is known that choosing F/M is dependent on fuel type, type and amount of metal cations to chelate, and the pH of the solution mixture [26]. If the F/M is low it may cause the complexation of the metal cations to be incomplete. This will have the possible consequence of a secondary phase forming.

when the F/M is too high it can lead to a decrease in the powder's crystallinity. Deganello, Marcì, and Deganello tested for the impact of F/M on the synthesis of $Sr_{0.85}Ce_{0.15}FeO_{3-x}$. They used a C/M of 2 and 4 and observed, through XRD, that when F/M is 2, almost 100 wt% perovskite is present after calcination. However, when the F/M is 4 the diffraction peaks of perovskite structure disappear [28].

Deganello, Marcì, and Deganello suggests that the disappearance of the perovskite-type pattern may be due to the formation of carbonates and oxides, produced by excess not-bounded citric acid, instead of forming multicomponent perovskite [28]. This is supported by Park et al. who made the same speculations that the residues hinder the formation of perovskite structure [29].

### 3.2.4 Effect of pH

The pH should be maintained at a slightly acidic level to avoid the formation of metal hydroxides and/or other salts. If not, The acidity comes from the metal salts dissolving in water where a hydrolysis reaction possibly occurs. Adjusting the pH is usually done by either adding acidic or alkaline species. However, an excess of either species in the solution may affect the structure morphology of the final product [27]. Deganello, Marcì, and Deganello synthesised $BaCe_{0.9}Y_{0.1}O_{3-x}$ and $Sr_{0.85}Ce_{0.15}FeO_{3-x}$ at pH 1, 4 and 6. At pH 1 the gel transformed into a brownish powder, and the auto combustion occurs when it reaches higher values of 250 °C. This occurs because, at low pH, citric acid is poorly dissociated, does not form any metal complexes, and further decomposes at 175 °C [28]. This is supported by similar results of Cannas et al. who analyzed cobalt ferrites [30].

### 3.2.5 Calcination

Calcination is a process where the perovskite is heated to a specific temperature to remove impurities such as excess citric acid and nitrates. Calcination can affect properties of the perovskites such as increasing the specific surface area and thereby increasing the catalytic effect. Kucharczyk et al., who synthesized $LaFeO_3$, found that the calcination temperature affected the physicochemical properties of the perovskite. Going from 650 to 850 °C caused a decrease in the BET-specific surface area of the perovskite even though the calcination time was reduced from 10 to 4 hours. It is also observed that the degree of crystallinity of the perovskite increased with temperature [31].
Naveenkumar et al. synthesized $SrFeO_3$ through SCS and calcined it at different temperatures to observe its effect. At lower temperatures than 600 °C, traces of $Sr(NO_3)_2$ were still observed but disappeared at higher temperatures. Above 600 °C traces of carbonates such as $SrCO_3$ were observed which can cause a decrease in the catalytic activity. At 900 °C no traces of $SrCO_3$ is were observed. At this temperature, the main diffraction pattern was $SrFeO_{3-\delta}$ with an indication of $Sr_4Fe_3O_{10-x}$ also present. From this, a higher calcination temperature is favorable for $SrFeO_3$ catalytic properties and causes fewer impurities [32].

## 3.3 Catalytic effect

Perovskites catalyze by gaining or releasing electrons in connection with redox reactions, which can happen by electrical conductivity through the B-site cations having different charges $B^{n+}$ and $B^{(n+1)+}$. This can be shown by the following equation **Equation 3.3**:

$$B^{n+} - O^{2-} - B^{(n+1)+} \rightarrow B^{(n+1)+} - O^{-} - B^{(n+1)+} \rightarrow B^{(n+1)+} - O^{2-} - B^{n+} \tag{3.3}$$

Through the equation above perovskites can release and obtain electrons and therefore act as catalysts. To increase the catalytic effect it would be favorable if the cation is unstable and therefore easy to jump between the two valence states [13].

Another way perovskites can gain and release electrons and act as a catalyst is through oxygen vacancies. Oxygen vacancies can be seen as a hole in the perovskite crystal structure where oxygen usually is found. The way oxygen vacancies occurs is when two $B^{(n+1)+}$ decreases $B^{n+1}$. This results in a charge difference forcing the oxygen out to even it out as seen from **Equation 3.4** :

$$B^{(n+1)+} - O^{2-} - B^{(n+1)+} \rightarrow B^{n+} - V_O^{\bullet\bullet} - B^{n+} + \frac{1}{2}O_2 \tag{3.4}$$

where $V_O^{\bullet\bullet}$ is an oxygen vacancy.
Another important factor that affects the catalytic effect is the specific surface area and particle size of the perovskites. This is because catalysis with perovskite is a surface reaction requiring great contact between the surface of the catalyst and the substrate. From this, the surface area is preferred to be large while the particle size should be smaller [33].

### 3.3.1 Catalytic methods

Perovskites have different ways of approaching the neutralization of organic pollutants. Some of the more modern techniques include photocatalysis And thermal catalysis with both showing advantages and disadvantages compared to each other. A disadvantage of photocatalysis is the need for sunlight meaning it either has to run in the day or a specific lamp is needed to run at night.

### 3.3.2 Thermal catalysis

As mentioned in **Chapter 1** an interesting way of neutralizing organic pollutants is through thermal catalysis under dark ambient conditions. Thermal catalysis is categorized as an AOP. It works by mineralizing pollutants into non-toxic/less toxic products such as $H_2O$, $CO_2$, and salts. Possible ROS that occur are $OH^{\bullet}, O_2^{\bullet}, HO_2^{\bullet -}$ and/or $SO_2^{\bullet -}$ generated in aqueous systems to mineralize the pollutants [1].

In general thermal catalysis, similar to classical heterogeneous catalysts such as photocatalysis, happens in five steps:
(1) the reactants are transferred from the fluid phase to the catalyst surface.
(2) The reactants are adsorbed onto the catalytic surface.
(3) The catalytic reaction occurs in the adsorbed phase.
(4) The products from the catalysis can now be desorbed from the catalytic surface.
(5) Now the product can be transferred from the interface region into the bulk solution [1].
When it comes to the mechanism of thermal catalysis in dark ambient conditions there is not a united front. Based on the literature the mechanism can be grouped into 4 different categories which include the Surface electron transfer mechanism, the Hopping conduction mechanism, the Mars-van Krevelen mechanism, and the Free radical chain autoxidation mechanism.
From **Equation 3.5** is shown what all the theories have in common, which is that the adsorption of the organic pollutant is very important because it allows the catalytic reaction to be fast and efficient [1].

$$Organic\ Pollutant + Catalyst \rightarrow Catalyst(Adsorption\ of\ Organic\ Pollutant) \tag{3.5}$$

**Surface electron transfer mechanism** For surface electron transfer mechanism 2 main things can occur. Either the electrons from the pollutants are injected into the catalyst by the conduction band or the catalyst surface redox pair initiates the generation of trapped electrons and a semi-oxidized radical cation. Trapped electrons are consumed by adsorbed oxygen creating anionic superoxide radicals $(O_2^{\bullet -})$. These are then protonated which leads to the formation of hydroperoxyl radicals $(HO_2^{\bullet})$ which eventually will form hydrogen peroxide. The hydrogen peroxide that is formed will then dissociate into hydroxyl radicals $(OH^{\bullet})$. The formation of singlet oxygen radicals is by radical interactions meaning that the ROS is behind the degradation of organic pollutants in the surface electron transfer mechanism [1, 34]. The general mechanism can be seen on **Figure 3.4**.

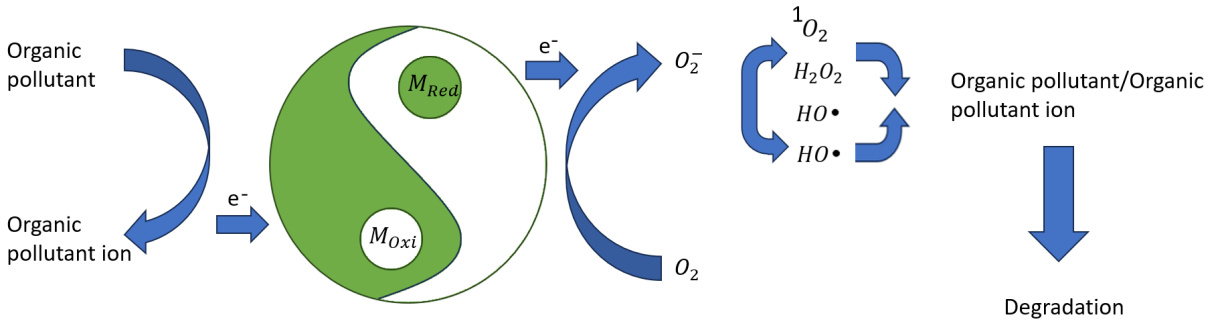


**Figure 3.4:** The figure illustrates the general surface electron transfer mechanism Inspired by [1]

**Hopping conduction mechanism** The Hopping conduction mechanism can generate ROS to attack organic pollutants. This happens when the catalyst receives energy equal to or higher than its band gap energy. This results in electrons in the valence band being excited into the conduction band creating positively charged holes in the valence band. These holes are highly oxidative and can cause the oxidation of $H_2O$ into hydroxyl radicals. Electrons are also able to be trapped by adsorbed oxygens causing the formation of ROS [1, 35].

**Mars-van Krevelen mechanism** The Mars-van Krevelen mechanism consists of 2 steps. The first step i the generation of a partially reduced catalyst. This happens when the pollutant is oxidized by a lattice of oxygen in the catalyst thereby reducing the catalyst as well. The reduced catalyst i is then able to be re-oxidized by $O_2$ as the second step [36]. ROS can be formed which will lead to the degradation process. This happens when the catalyst lattice oxygen is activated forming active oxygen and an oxygen vacancy [1]. When it comes to the rate of degradation, oxygen transfer between the catalyst and pollutant is said to be the rate-determining step [1].

**Free radical chain autoxidation mechanism** For free radical chain autoxidation, the overall steps include initiation, chain carrier formation, propagation, and termination. The initiation happens when the catalyst reacts with the organic pollutants transforming them into radicals (See **Equation 3.6**). The catalyst can regenerate itself through re-oxidization by adsorbing $O_2$ (See **Equation 3.7**). This generates an oxygen radical which eventually will become a hydroxide radical. These radicals are used in the second initiation step which generates a radical and water(See **Equation 3.8**). The radical can then react with $O_2$ creating a peroxy radical that acts as the chain carrier, hence the step is called chain carrier formation (See **Equation 3.9**). The peroxy radical can then abstract a hydrogen atom from the organic pollutant causing propagation and another radicalization of the organic pollutant (See **Equation 3.10**). An alternative to this is termination where 2 peroxy radicals combine creating ROO-OOR and thereby terminating the reaction(See **Equation 3.11**) [1, 37].

$$RH + Cat \rightarrow R^{\bullet} + H^{+} + Cat_{Red} \tag{3.6}$$

$$Cat_{Red} + O_2 \rightarrow Cat + O_2^{\bullet} - \tag{3.7}$$

$$RH + OH^{\bullet} \rightarrow R^{\bullet} + H_2O \tag{3.8}$$

$$R^{\bullet} + O_2 \rightarrow ROO^{\bullet} \tag{3.9}$$

$$RH + ROO^{\bullet} \rightarrow ROOH + R^{\bullet} \tag{3.10}$$

$$2ROO^{\bullet} \rightarrow ROOOOR \tag{3.11}$$

# Chapter 4
# Method

## 4.1 Chemicals

For the synthesis of doped and pure $SrFeO_3$, strontium nitrate, iron(III) nitrate nonahydrate, zinc nitrate hexahydrate, nickel nitrate hexahydrate, citric acid, ammonium nitrate, ammonium hydroxide, and copper nitrate trihydrate.

## 4.2 Synthesis of strontium ferrate

Doped and pure $SrFeO_3$ was prepared by weighing the chemicals on a Mettler AM100 weight. The weight of the chemicals can be found in **Appendix B**). Firstly strontium nitrate, iron(III)nitrate nonahydrate, and either copper nitrate trihydrate, nickel nitrate hexahydra, or zinc nitrate hexahydrate were dissolved in 190 mL of demineralized water under magnetic stirring. When dissolved, citric acid is added. When the citric acid is dissolved, ammonium nitrate is added to the solution. The pH is then adjusted to approximately 3.14 with ammonium hydroxide.
The solution is then heated to 80 °C to evaporate the water. When the evaporation has occurred and a gel-like substance is left the thermometer is removed and the temperature is set to 250 °C to rapidly increase the temperature and begin the self-ignition process. The procedure can be seen in **Figure 4.1**. The powder was then calcined at 1000 °C at a rate of 10 $\frac{^\circ C}{minutes}$ for 5 hours and cooled overnight.

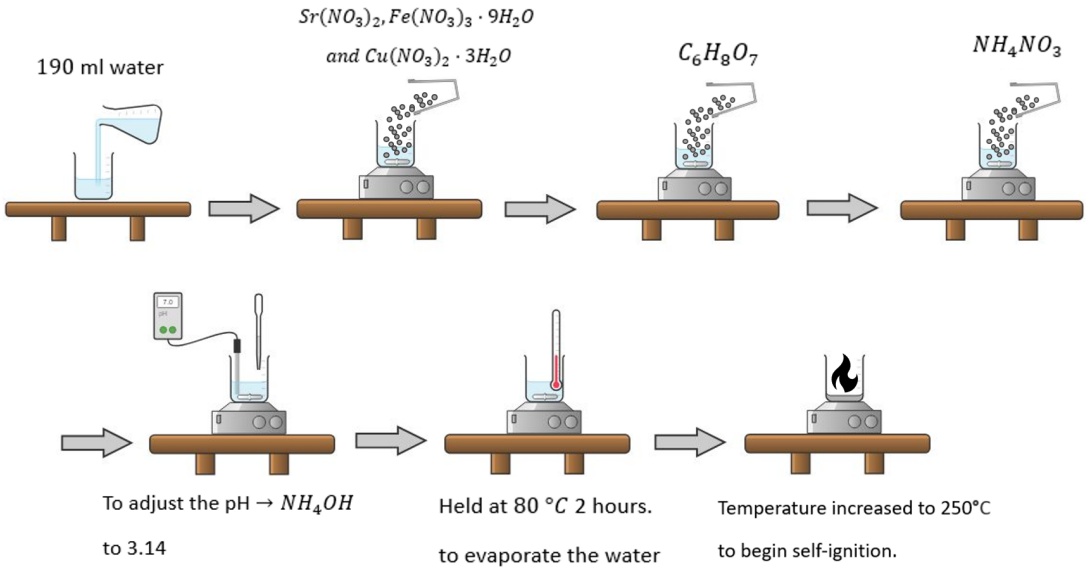


**Figure 4.1:** The figure illustrates the chemical procedure of the synthesis. The figure is made in chemix.org

## 4.3 Characterization of perovskites

The perovskites were characterized through XRD and XPS to confirm single-phase perovskites and to characterize the surface chemistry of the perovskite.

### 4.3.1 XRD

The perovskites were analyzed through XRD to confirm single-phase perovskites. All the X-ray diffraction measurements were performed on an Empyrean PANalytical diffractometer with $Cu - K_\alpha$ a step size of 0.013. The measurements were done at 40 mA and 45 kV.
The XRD spectrums were analyzed with Rietveld refinement using the program GSAS-II. The phases used to analyze the perovskites were $Sr_3Fe_8O_{23}$ and $Sr_4Fe_4O_{11}$ which were provided by the supervisor. The refinement type was analytic hessian with a max cycle of 15. A Chebyschev polynomial function was used with 7 coefficients. The unit cell was refined and for the structure refinement, phase fraction, microstrain, and crystalize size were considered as variable parameters.

### 4.3.2 XPS

X-ray photoelectron spectroscopy (XPS) measurements were performed using a Specs XR50 with a non-monochromatic Al Kα (1487 eV) X-ray source and a Phobos 1501D-DLD electron detector. The data was analyzed in CasaXPS software. The background used for O1s and Sr3d was Shirley. The Shirley background removed a large amount of the Fe2p data so the linear background was applied.

## 4.4 Thermal catalysis

To investigate the degradation properties of $SrFeO_3$, thermal catalysis was performed. This was done by firstly making a 100 $\frac{mg}{L}$ stock solution which had its pH altered down to 2 using HCl. Then a liter of 5 $\frac{mg}{L}$ were made from the stock solution to have enough for the experiment. 200 ml of the 5 $\frac{mg}{L}$ were transferred to a 250 ml bluecap which has been covered in tin foil to create dark ambient conditions. The solution is then heated to the desired temperature (20°C, 35°C, 45°C, 55°C). When the desired temperature is achieved, 1 $\frac{g}{L}$ perovskite is added to the solution and the experiment begins when the perovskite is somewhat evenly spread. Samples are taken frequently in the beginning and with a bigger gap later on. A sample is taken at the following times: 0, 1, 2, 5, 10, 15, 30, 60, 90 min. every sample is then measured on a full spectrum with a "Varian Cary bio 50" UV-Vis spectrophotometer between 300-700 nm.

## 4.5 Recycling

To test the perovskite's effectiveness when exposed to multiple cycles of Rh-B solution recycling experiments were performed. It is done at 45 °C for 1 hr to make sure that all the Rh-B is gone or converted into a different molecule. Each sample consisted of 5 ml solution resulting in 160 ml remaining after each cycle. Afterward, 40 ml of a 25 $\frac{mg}{L}$ Rh-B solution was added to regain a concentration of 5 $\frac{mg}{L}$ and 200 ml. This is done 3 times completing a cycle of 4. The data is collected as a UV-Vis full spectrum in the range of 300-700 nm using the same spectrophotometer as mentioned above.

### 4.5.1 AAS

For each metal analyzed, copper, iron, and strontium, a standard curve was produced where the wavelength is dependent on the metal analyzed and the concentration of the samples. The standard curve is diluted in 0.1 M $HNO_3$ whereas 50 µl 7 M $HNO_3$ is added to the analyte. Due to complications with finding the right standard-curve concentration for iron, copper, and strontium, the samples were diluted with a factor of 7, 3, and 30 respectively. Analyzing the iron concentration the wavelength of 302.1 nm was used. Analyzing the strontium concentration the wavelength of 460.7 nm was used. Analyzing the copper concentration the wavelength of 324.8 nm was used.

# Chapter 5
# Results

## 5.1 Characterization

### 5.1.1 XRD

After the perovskite synthesis, XRD was done on all the samples to verify a single-phase compound. From **Figure 5.1** the XRD patterns for the synthesized perovskites are shown. The main peak is associated with the formation of the desired perovskite however, in some cases, a small peak, shown by the arrow, can be observed. This only occurred if the samples were either doped with nickel or zinc. Palma et al. saw similar peaks which they attributed to the layered tetragonal perovskite of $Sr_3Fe_2O_{7-\delta}$ [10]. These additional peaks create an issue as they confirm the double-phase structure when using nickel and zinc as dopants. This makes it difficult to determine which part of the perovskites is doing the degradation process. As a result, copper doping, which showed characteristic peaks, is the doping analyzed further.

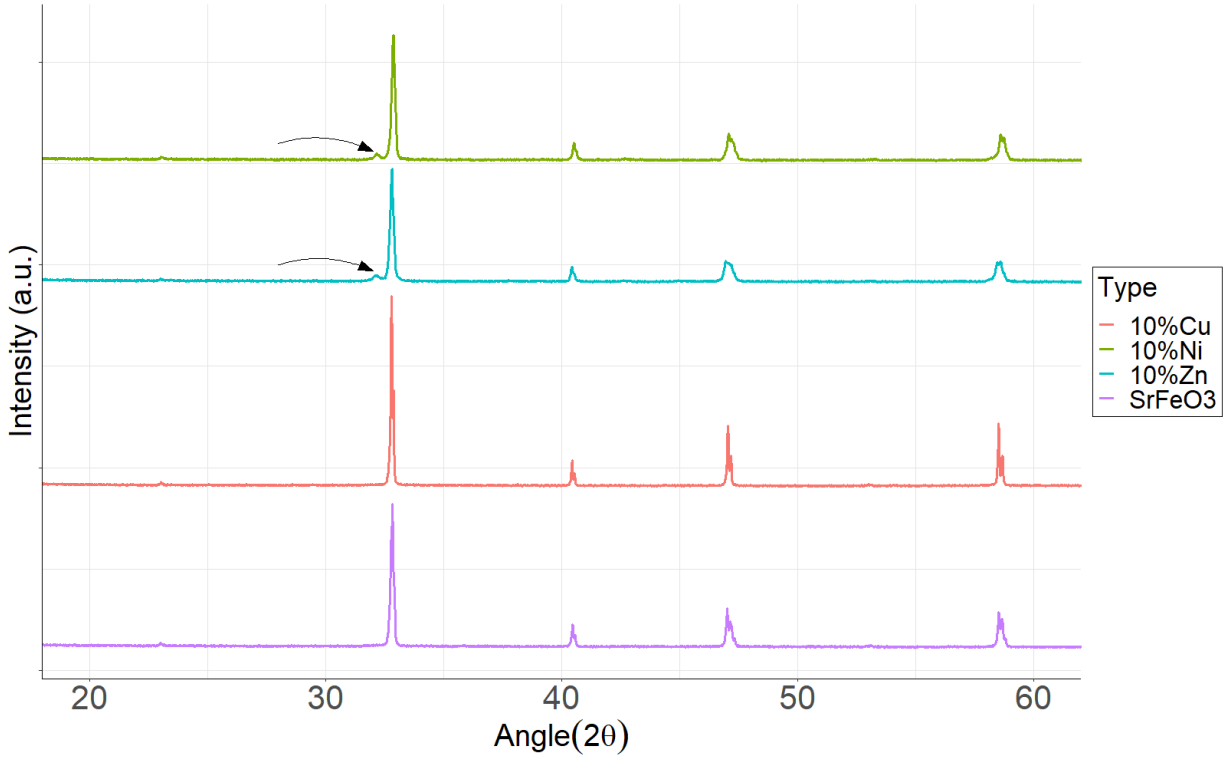


**Figure 5.1:** XRD patterns of all synthesized perovskites at 10% doping and a pure $SrFeO_3$.

Rietveld refinements were performed to confirm if the synthesized perovskite resembles the literature. The refinements were done on all pure and copper doped $SrFeO_3$ through GSAS-II with the tetragonal phase of $Sr_8Fe_8O_{23}$ ($\delta = 0.125$). However, this led to the issue of obtaining

a crystal size of 10000 nm for multiple perovskites, which is the maximum limit for GSAS-II, indicating inconsistent results.
As a result, an orthorhombic phase of $Sr_4Fe_4O_{11}$ ($\delta = 0.25$) was used which showed improved data when comparing $Chi^2$ and goodness of fit (GoF). **Table 5.1** show the average values of crystal size, microstrain, $Chi^2$, and GoF for each synthesized perovskite when using the orthorhombic phase.

**Table 5.1:** Overview of refinement data. * indicates the first phase that is used.

| Copper % | Crystalsize (nm) | Microstrain | $Chi^2$ | GoF | $Chi^{2*}$ | $GoF^*$ |
|---|---|---|---|---|---|---|
| 0% | $407.37 \pm 16.86$ | $1252 \pm 119.82$ | $2.59 \pm 0.10$ | $1.61 \pm 0.04$ | $2.59 \pm 0.10$ | $1.61 \pm 0.04$ |
| 1% | $343.73 \pm 21.27$ | $1193.40 \pm 282.94$ | $2.48 \pm 0.16$ | $1.58 \pm 0.05$ | $2.42 \pm 0.14$ | $1.56 \pm 0.04$ |
| 2.5% | $6211.27 \pm 4283.74$ | $2809.30 \pm 194.99$ | $2.16 \pm 0.32$ | $1.47 \pm 0.11$ | $2.26 \pm 0.48$ | $1.50 \pm 0.16$ |
| 5% | $827.67 \pm 558.62$ | $2126.93 \pm 650.93$ | $2.92 \pm 0.11$ | $1.71 \pm 0.03$ | $2.93 \pm 0.12$ | $1.72 \pm 0.04$ |
| 10% | $498.47 \pm 50.37$ | $600.46 \pm 48.07$ | $4.31 \pm 0.10$ | $2.07 \pm 0.09$ | $10.69 \pm 0.36$ | $3.44 \pm 0.36$ |

The obtained crystal size of roughly 500 nm found through the new phase is similar to what is found in the literature [38]. The crystal size of $SrFeO_3$ with a copper content of 2.5% is significantly higher than the rest assizes of 1572.9, 7070.9, and 10000 nm were obtained which averaged a crystal size of 6211.27 nm. This trend was also observed when using the tetragonal phase and in general, can not be reasonably explained. $SrFeO_3$ doped with 5% copper also shows slightly higher values. This is due to one of the refinements showing a crystal size of 1472.7 nm while the rest were around 500 nm. This trend was also seen when refining with a tetragonal phase, which is unreasonable and can therefore not be explained. A noteworthy mention is that the perovskite having a crystal size of 1472.7 nm was not used for thermal catalysis meaning that it did not influence further work. It can be observed in the table that the $Chi^2$ and GoF are for the most part close between the two phases. However, the 10% copper doped $SrFeO_3$ shows significantly lower values when using the orthorhombic phase instead of the tetragonal phase. This indicates that more oxygen vacancies are present as it is more likely that the synthesized perovskite is orthorhombic than tetragonal. The orthorhombic structure of $SrFeO_3$ is supported in literature as Kumar et al. saw similar structure through Rietveld refinement [39].

### 5.1.2 XPS

**Figure 5.2** illustrates the O 1s, Fe 2p, and Sr 3d region of the samples with binding energy values, and the relative abundance of the different components is shown in **Table 5.2**. A detail worth mentioning is that a general displacement occurs for most of the binding energies when compared to literature [24, 40]. The reason for this displacement is unknown, however, the distribution of peaks of the different compounds still resembles what is found in literature and acceptable comparability is assumed.

XPS measurement of O 1s region shows two characteristic components **see Figure 5.2a**. The peak with the lowest binding energy (approx. 534 eV) indicates oxygen in the lattice ($O_L$) whereas the higher binding energy peaks would indicate adsorbed oxygen and/or possible carbonates ($O_{ads}$) [40]. The ratio of $\frac{O_L}{O_{ads}}$ is an indication of oxygen vacancies. Pure $SrFeO_3$ showed the highest ratio resulting in the lowest amount of oxygen vacancies present in the perovskite structure. An observation is that the ratio drops with the increasing copper content indicating an increase in oxygen vacancies. Comparing this to the refinement of the perovskite

no correlation can be observed between oxygen vacancies and the stability of the perovskite. However, the orthorhombic phase shows a significantly better fit for 10% copper which could indicate that the oxygen vacancies increase.

Analyzing the Fe 2p (**See Figure 5.2b**) two main peaks occur around 713 eV and 715 eV. The peak with the lowest binding energy indicates the presence of $Fe^{3+}$-ions whereas the highest indicates $Fe^{4+}$-ions. When looking at the table in **Table 5.2**, an increase in $Fe^{4+}$-ions occurs as the copper content increases. This is due to $Fe^{4+}$-ions trying to neutralize the change in charges when a $Cu^{2+}$-ion substitutes an iron ion.

| Sample | O1s | Fe2p | Sr3d |
|---|---|---|---|
| 0% | 534 (36.72%) ($O_{ads}$)<br>533 (63.28%) ($O_L$) | 713 + 715.7 + 726.8 (78.85% $Fe^{3+}$)<br>715.7 + 730.4 (21.15% $Fe^{4+}$) | 135.8 + 137.6 (55.42% $Sr_{OH/CO_3}$)<br>134.1 + 136.1 (44.58% $Sr_L$) |
| 1% | 534.4 (44.55%) ($O_{ads}$)<br>532.7 (55.45%) ($O_L$) | 713 + 717.6 +726.8 (77.99% $Fe^{3+}$)<br>715.4 + 728.6 (22.01% $Fe^{4+}$) | 137.7 + 135.8 (48.91% $Sr_{OH/CO_3}$)<br>134.5 + 136.4 (51.09% $Sr_L$) |
| 5% | 533.7 (51.45%) ($O_{ads}$)<br>532.7 (48.55%) ($O_L$) | 712.7 + 721.1 + 726.2 (77.44% $Fe^{3+}$)<br>715.9 + 729.4 (22.56% $Fe^{4+}$) | 135.5 + 137.5 (48.9% $Sr_{OH/CO_3}$)<br>134.1 + 136.1 (51.1% $Sr_L$) |
| 10% | 532.9 (79.58%) ($O_{ads}$)<br>530.6 (20.42%) ($O_L$) | 711.9 + 719.7 + 725.6 (70.29% $Fe^{3+}$)<br>714.5 + 728.4 (29.71% $Fe^{4+}$) | 133.8 + 137.5 (23.24% $Sr_{OH/CO_3}$)<br>133.6 + 135.5 (76.76% $Sr_L$) |

**Table 5.2:** XPS data based on CasaXPS measurements.

The increase $Fe^{4+}$-ions as copper concentration increases are in agreement with literature [25]. Sun et al. also saw a similar trend for the ratio of $\frac{O_L}{O_{OH}}$ as it decreased with increased copper concentration resulting in more oxygen vacancies. However, this trend is unreasonable as the increase in $Fe^{4+}$-ions should lead to fewer oxygen vacancies trying to balance additional positive charges. An observation made comparing $Fe^{4+}$-ion content with the literature is that in this project it is significantly lower [25]. This trend is unable to be explained without further analysis and is unfortunate as the aim of copper doping is to increase $Fe^{4+}$ content.

XPS measurements for Sr 3d can be seen in **Figure 5.2c**. Two main components are detected here around 136 eV ($Sr_{OH/CO_3}$) which is an indication of strontium in the $SrCO_3$ structure whereas the peak detected around 134 eV ($Sr_L$) indicates the presence of strontium in the lattice. As the concentration of copper increased the proportion of $SrCO_3$ decreased which in theory indicates that the catalytic effect of the perovskite would increase as less strontium is in carbonate form possibly blocking the catalytic sites.

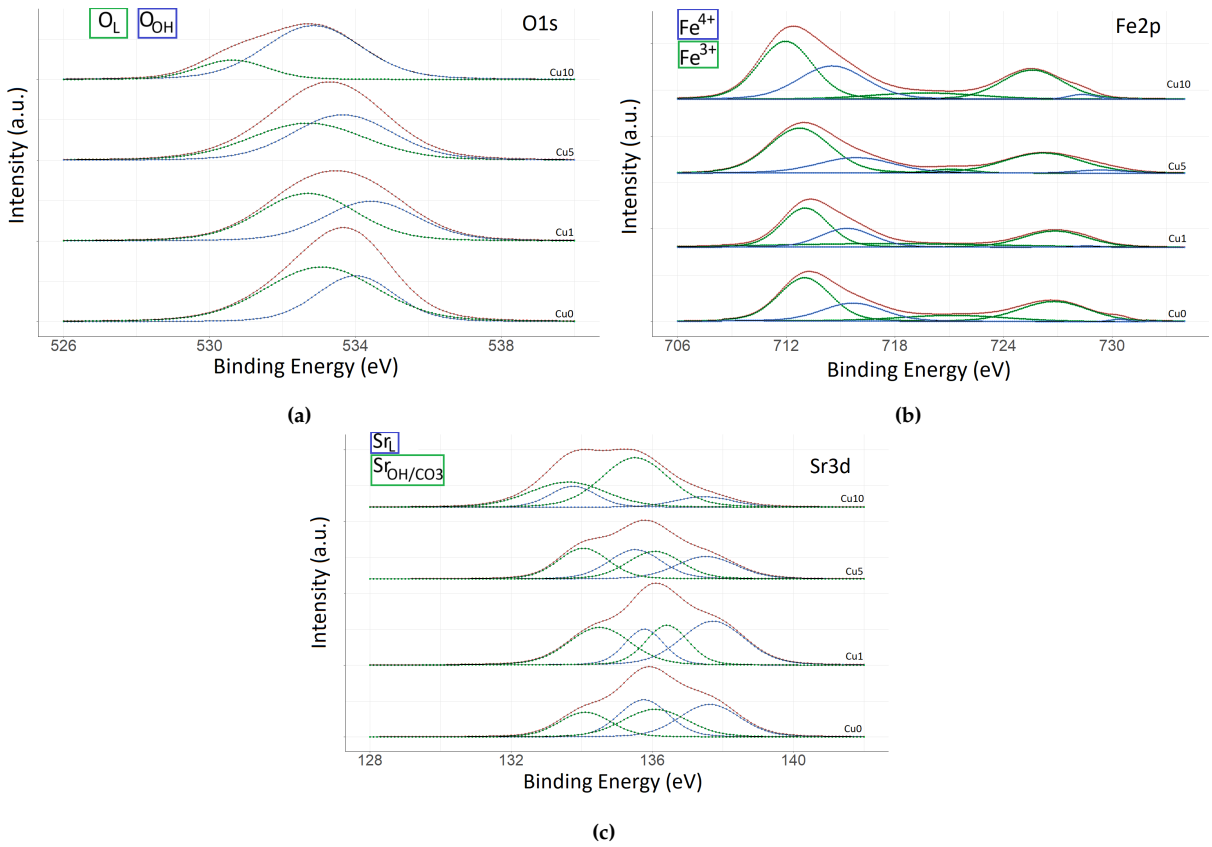


**Figure 5.2:** XPS spectra of investigated samples: (a) O 1s region; (b) Fe 2p region; (C) Sr 3d region.

## 5.2 Thermal catalysis

The progress of creating a standard curve can be found in **Appendix A**.

### 5.2.1 Degradation of Rhodamine B

To make sure that no other factors than the perovskite degrades the Rh-B, a solution was made of 5 $\frac{mg}{L}$ Rh-B without the addition of perovskites and heated to 25°C (**see Figure 5.3**).

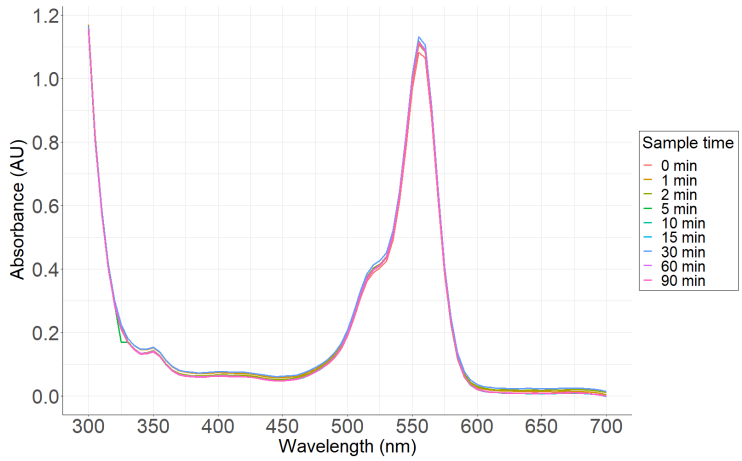


**Figure 5.3:** The figure shows the full spectrum of Rh-B over 90 min at 25°C without adding perovskite to the solution.

It can be observed that no degradation or change in the Rh-B occurs. A weird shift can be seen at roughly 325 nm for the sample taken at 5 minutes which is assumed to be an error made by the spectrophotometer. An increase in absorbance can be observed around 550 nm which was not expected because no Rh-B was added during the experiment. An explanation for this could be that the cuvette gained a very light pink color after multiple measurements. This could lead to an increase in absorbance even though no Rh-B was added during the experiment.

From **Figure 5.4** the degradation of Rh-B with $SrFeO_3$ as the acting catalyst at different temperatures can be observed. A clear trend can be seen in that a higher temperature leads to faster and more effective degradation of Rh-B. This trend is observed for all the explored copper content concentrations (**see C.1**). A control sample was made with Rh-B with no addition of perovskites to confirm that the perovskites are responsible for the degradation. The figure shows no decrease in Rh-B concentration, indicating that the perovskite is responsible for the degradation. The increased reaction rate is expected due to particles moving faster at higher temperatures, resulting in more collisions and a faster reaction. Not only does the frequency of collisions increase, but also the effectiveness of the collisions [41].

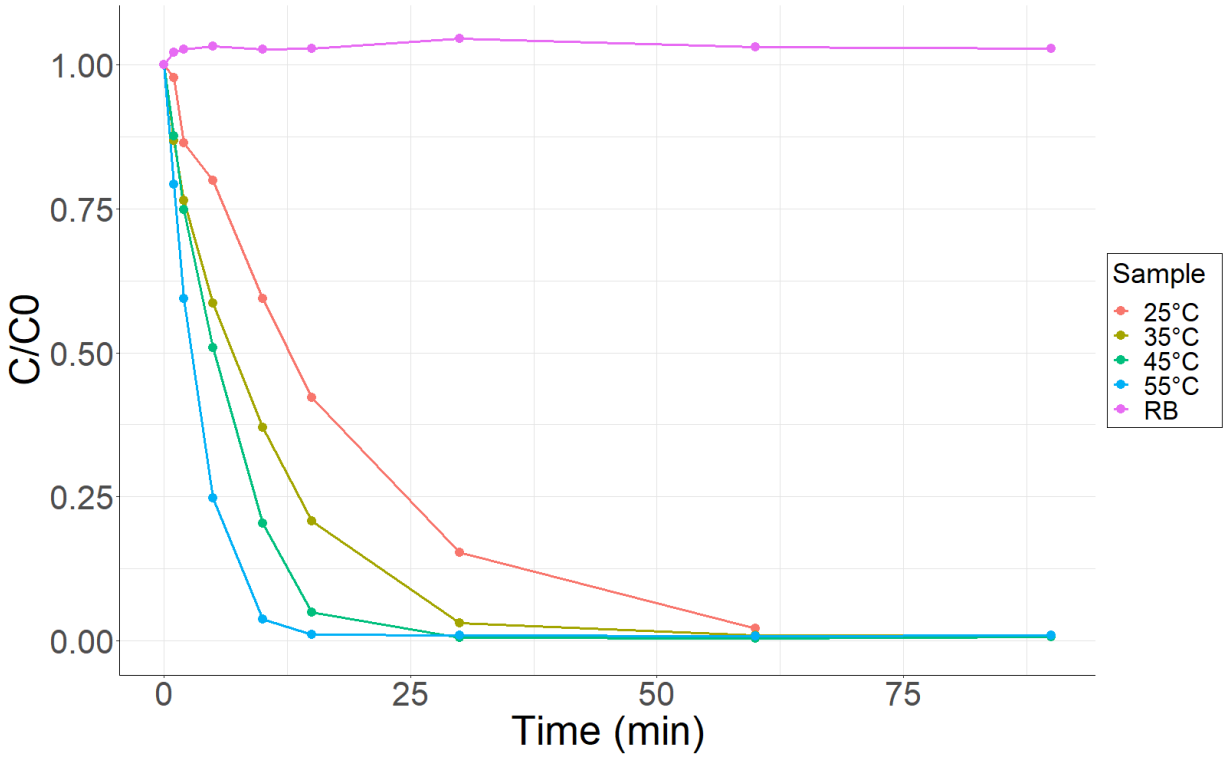


**Figure 5.4:** Degradation of Rh-B with $SrFeO_3$ as acting catalyst at different temperatures.

$\frac{C}{C_0}$ was plotted against time for all synthesized perovskites at 45°C to observe a possible correlation between copper content and degradation efficiency (see **Figure 5.5**). However, no such correlation is observed as the remaining temperatures saw a different doping % being the most efficient (**see C.2**).

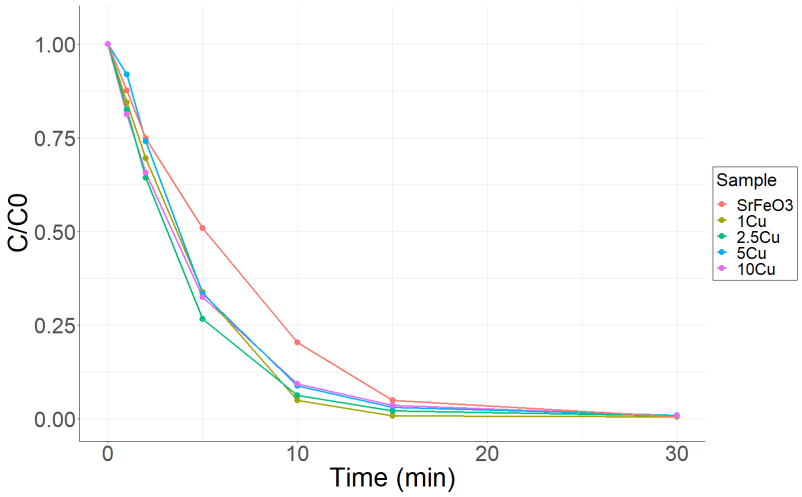


**Figure 5.5:** Degradation of Rh-B at 45° C

The reaction kinetics were determined through the differential method. From **Figure 5.6**, a clear correlation can be seen between ln[A] and time confirmed by a high $R^2$-value of 0.9986. The 0. and 2. order reactions are also illustrated with a significantly lower $R^2$-value, further indicating that the reaction follows a 1. order reaction. This is in agreement with literature which also observes a 1. order reaction when degrading an organic pollutant with doped $SrFeO_3$ as a catalyst [9, 11, 42].

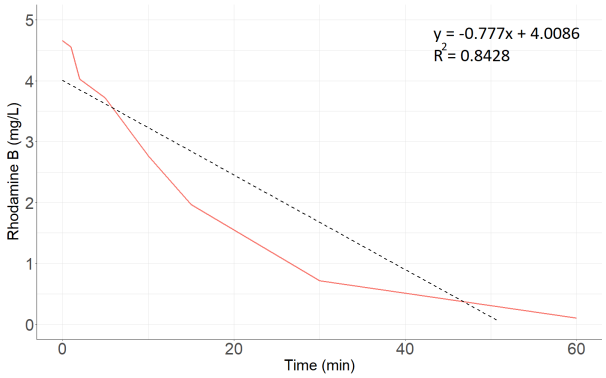


**(a)** 0. order kinetics

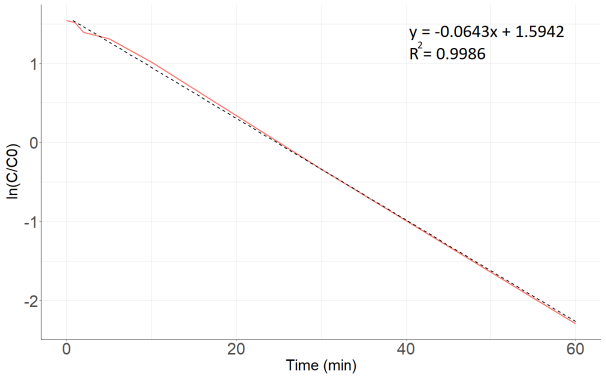


**(b)** 1. order kinetics

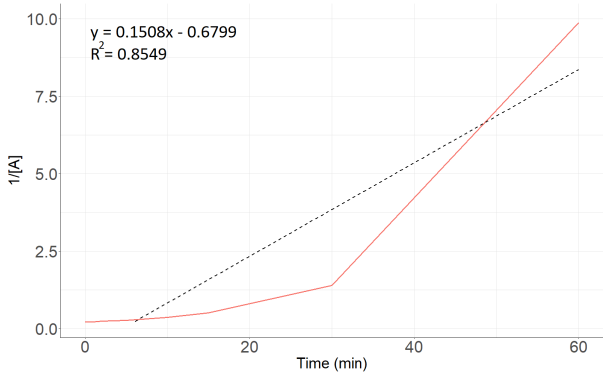


**(c)** 2. order kinetics

**Figure 5.6:** The figures illustrate fits for 0, 1, and 2. order kinetics

Commenting on the effect copper has on the rate constant, **Figure 5.7**, indicates no clear correlation. However, an increase in the rate constant is observed with increasing temperatures as expected. When fitting the rate to a 1. order reaction the $R^2$-values lie between 0.999-0.806 with the majority closer to 0.999 making reasonable fits. This means that the rate of the reaction is proportional to the concentration of the reactants. The table with all values can be found in **Table D.1**.

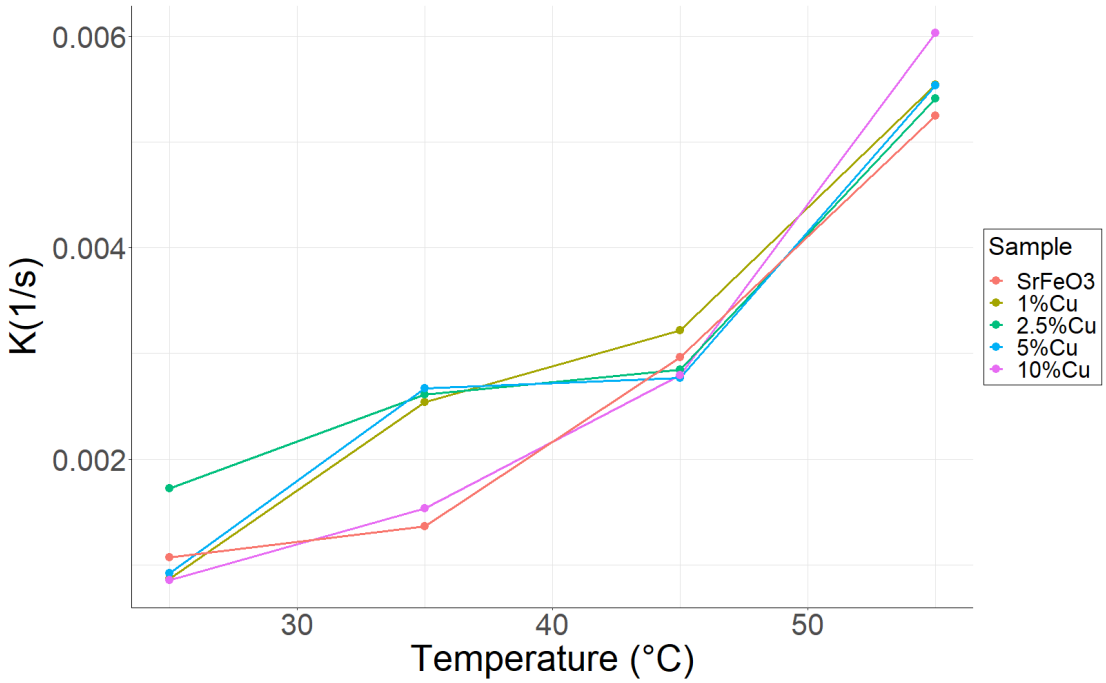


**Figure 5.7:** The rate constant as a function of temperature.

### 5.2.2 Activation energy

The activation energy can be found through the so-called Arrhenius equation (**Equation 5.1**).

$$k = Ae^{\frac{-E_a}{RT}} \tag{5.1}$$

from **Figure 5.8** it illustrates how a decrease in activation energy occurs with higher copper content. This trend stops at 5% copper having a minimum activation energy and 10 % copper having the highest activation energy. The activation energy was expected to decrease with copper content in theory should increase its catalytic effect which can be an indication that the reaction needs less energy to occur. 10 % copper having the highest activation energy could be an indication that it exceeds the beneficial limit for decreasing Rh-B.

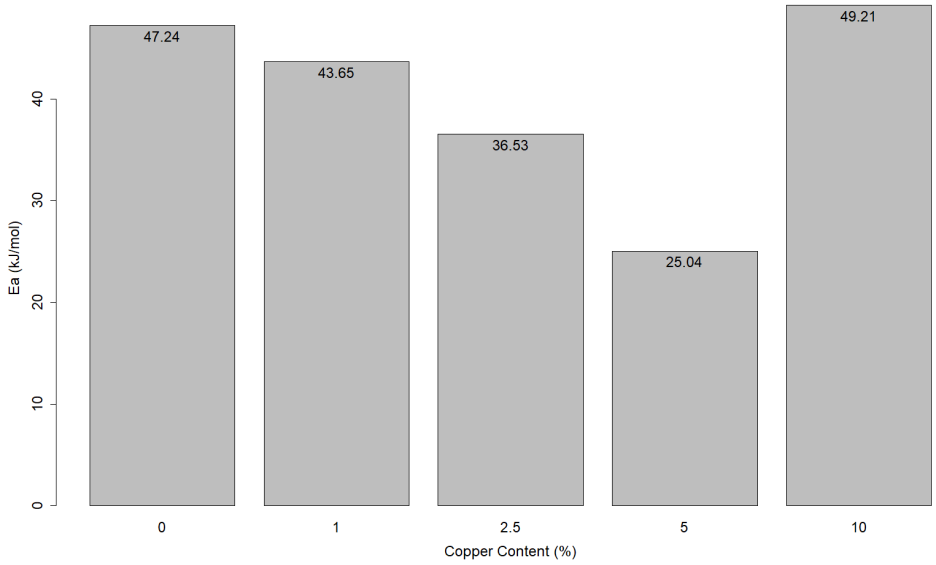


**Figure 5.8:** Activation energy as a function of copper content.

### 5.2.3 Recirculation

From **Figure 5.9** the degradation of Rh-B over 4 hours can be seen. An observable trend is that $SrFeO_3$ is not able to degrade it as effectively as the rest of the perovskites after 4 recycles. This could be an indication of copper doping increasing the degradation of Rh-B. An unfortunate trend that can be observed is the time of degradation slows down and for some of the perovskites, 1 hour is not enough time to degrade all the newly added Rh-B.

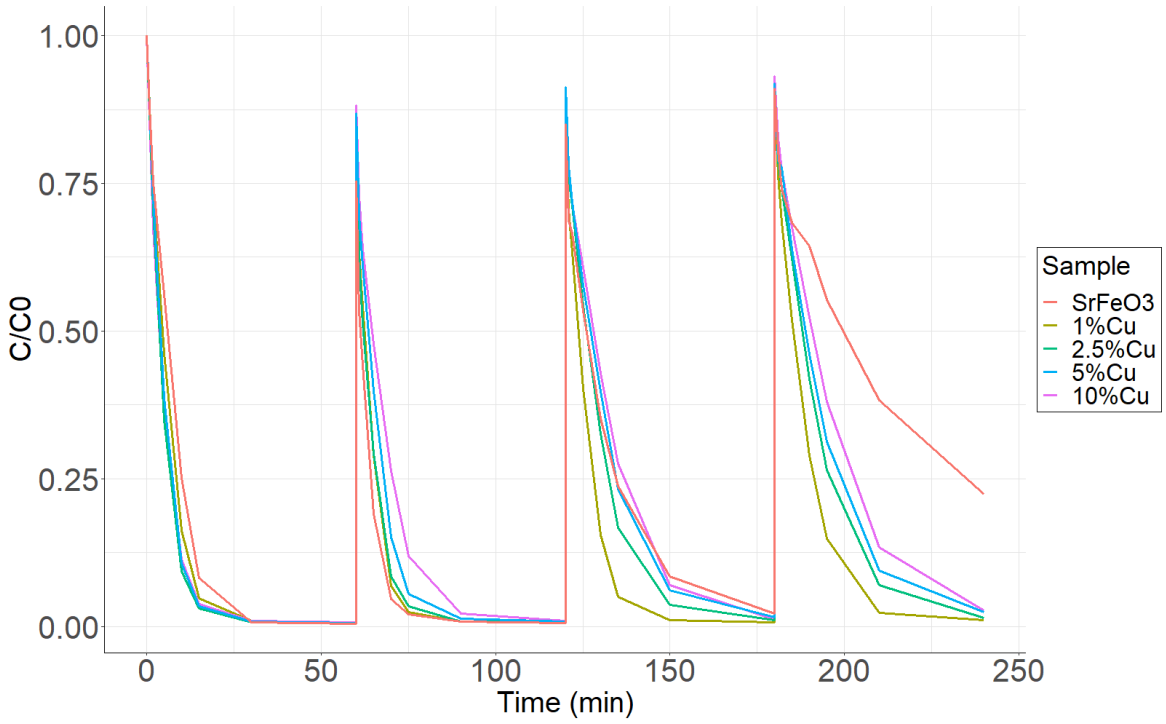


**Figure 5.9:** Ilustrating the degradation of Rh-B for each perovskite over 4 hours.

**Figure 5.10** illustrated a comparison between 4th recirculation of pure $SrFeO_3$ and 10% copper doped. A clear difference can be observed in that a blue shift happens from Rh-B's original peak at 555 mm to a new peak visual around 500 nm. This new peak can be seen growing with the increase of copper content in the perovskite.

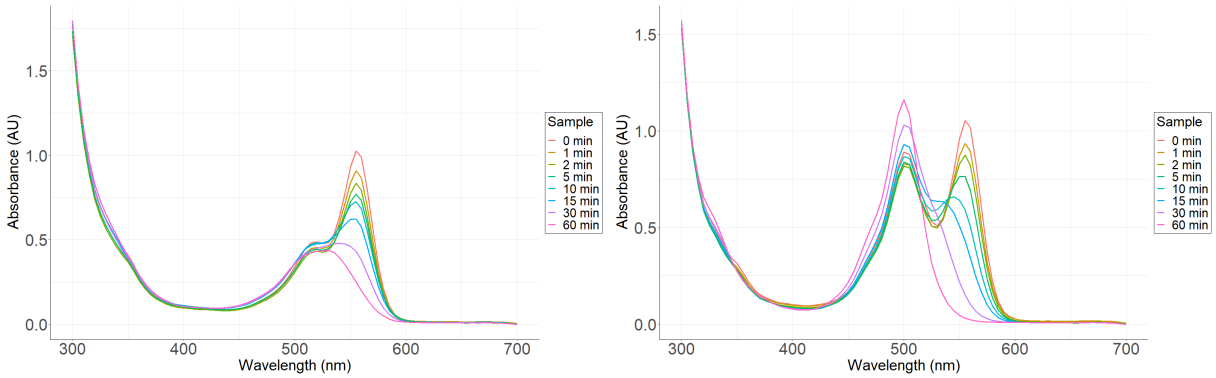


**(a)** 4th recirculation for Degradation of Rh-B with $SrFeO_3$ **(b)** 4th recirculation for Degradation of Rh-B with 10% copper

**Figure 5.10:** Comparison of recirculation for degradation of Rh-B

An observation that was made during the experiment was that with the addition of copper, the liquid post-experiment had a green color (**See Appendix F**). This green color was more potent with the increase in copper concentration in the perovskite which is in agreement with the UV-vis measurement as the peak at 500 nm intensifies at higher copper content. A possible explanation for the hypsochromic shift could be the *N*-deethylation of Rh-B. The product *N*-deethylation of Rh-B is called Rh-110 (**See Figure 5.11**).

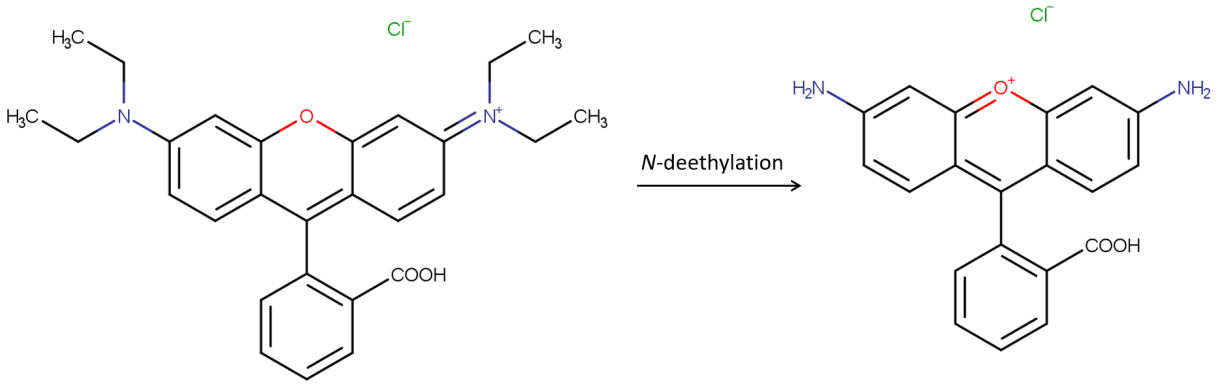


**Figure 5.11:** *N*-deethylation of Rh-B to Rh-110.

Rh-110 has a green color and also shows a peek around 500 nm when measuring its absorbance, which is very similar to what is found in this report. Literature reports on the conversion of Rh-B to Rh-110 through photocatalysis [43, 44]. Spilarewicz-Stanek et al. found a nearly identical UV-vis spectrum of Rh-B degradation into Rh-110 which similarly went from a pink color to a green liquid. As mentioned earlier in 3.3.2 Photocatalysis and thermal catalysis under dark ambient conditions are both included in heterogeneous catalysis and therefore the mechanisms are very similar. Thus the degradation of Rh-B into Rh-110 is a plausible explanation as to why a green liquid results from these experiments [43].

From **Figure 5.12** a general decrease in k-value is seen with pure $SrFeO_3$ and 1% copper doped an exception for second recirculation. The overall trend is an indication of weakening in the perovskites catalytic effect on the degradation of Rh-B. This is an unfortunate but expected trend and could be related to the leaching and release of metals into the solution. Leaching is one of the possible mechanisms of deactivation of the catalyst.
Another deactivation mechanism occurring could be catalyst poisoning. The catalyst poisoning most commonly happens through the carbonate formation of $SrCO_3$. Østergaard et al. explains that $SrCO_3$ is a commonly formed in $SrFeO_3$-based perovskites because of strontium's high affinity for atmospheric $CO_2$ [40]. The formation of carbonates is therefore a plausible explanation as to why the catalytic effect weakens during use.

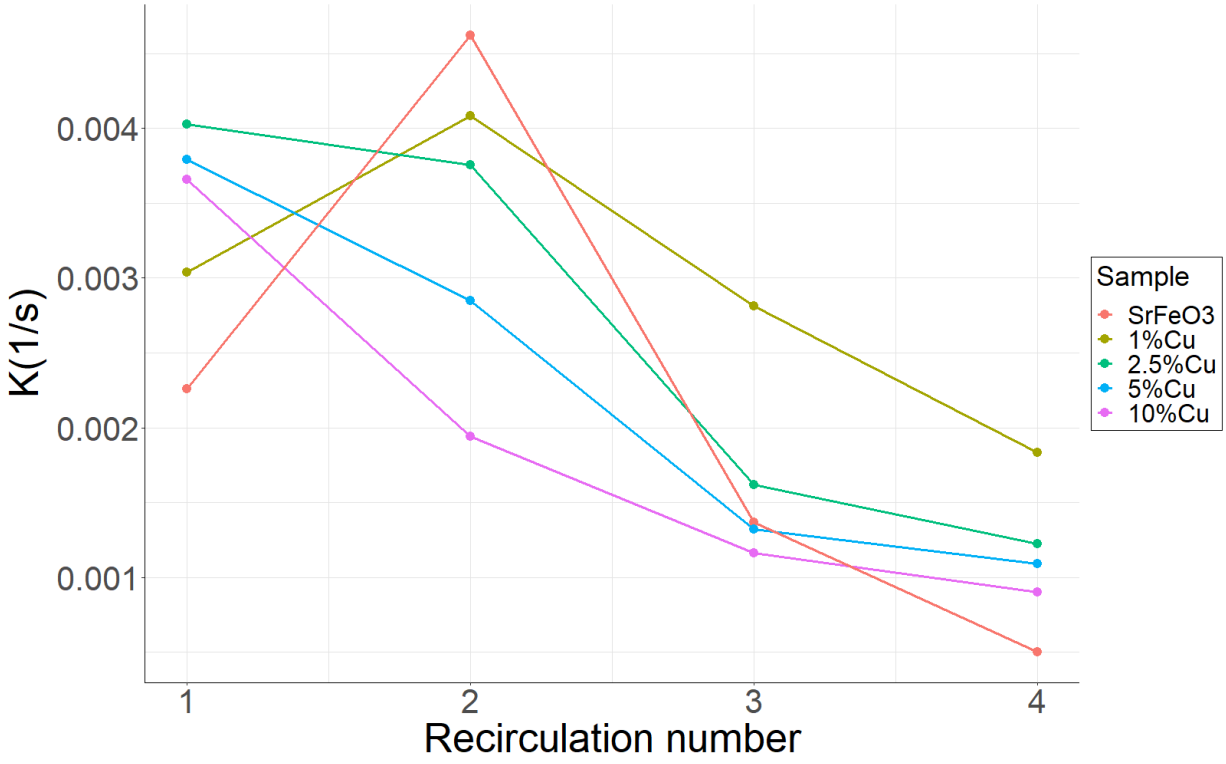


**Figure 5.12:** The rate constant after each cycle for different copper content.

The degradation of Rh-B was a general success in the beginning of degradation experiments. From **Appendix G** it can be observed that a full degradation of Rh-B for the first cycle of the experiment. The possible mechanism for this degradation involves 4 steps: 1) *N*-deethylation, 2) cleavage of chromophores (aromatic rings) 3) ring-openings, and 4) mineralization of the dye [45]. This can be observed in **Figure 5.13**.

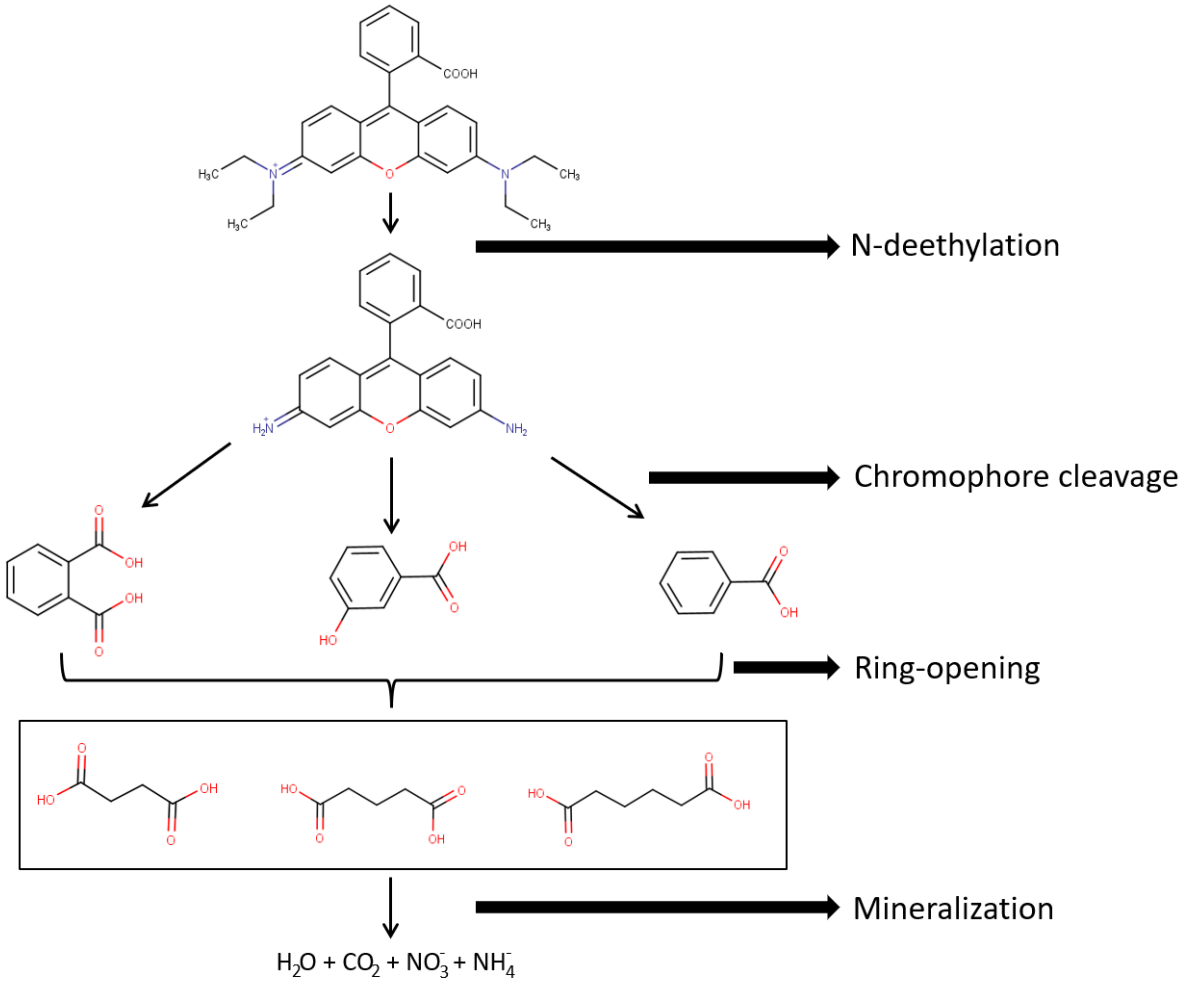


**Figure 5.13:** Possible degradation process of Rh-B. Inspired by [45]

## 5.3 Leaching of metals

From **Figure 5.14** the leaching of metals into the Rh-B solution during thermal catalysis is shown for all possible metals. The trend is similar throughout all measurements with an increase at 1% copper followed by a general decrease in strontium and iron concentration (see **Figure 5.14a and Figure 5.14b**). The copper concentration can be seen to continuously increase with the doping percentage of the perovskite (see **Figure 5.14c**). This trend is expected as a higher doping percentage increases the amount of possible copper leaching. A decrease in iron concentration as the copper content increases was also expected due to the perovskite having less iron capable of leaching. The trend of strontium having the highest amount of leaching is supported by literature. Palma et al. investigated cerium doped $SrFeO_3$ as a thermal catalyst for wastewater removal and found strontium to cause the highest amount of leaching from the perovskite followed by iron and cerium at a pH-value of 2.37 [10].

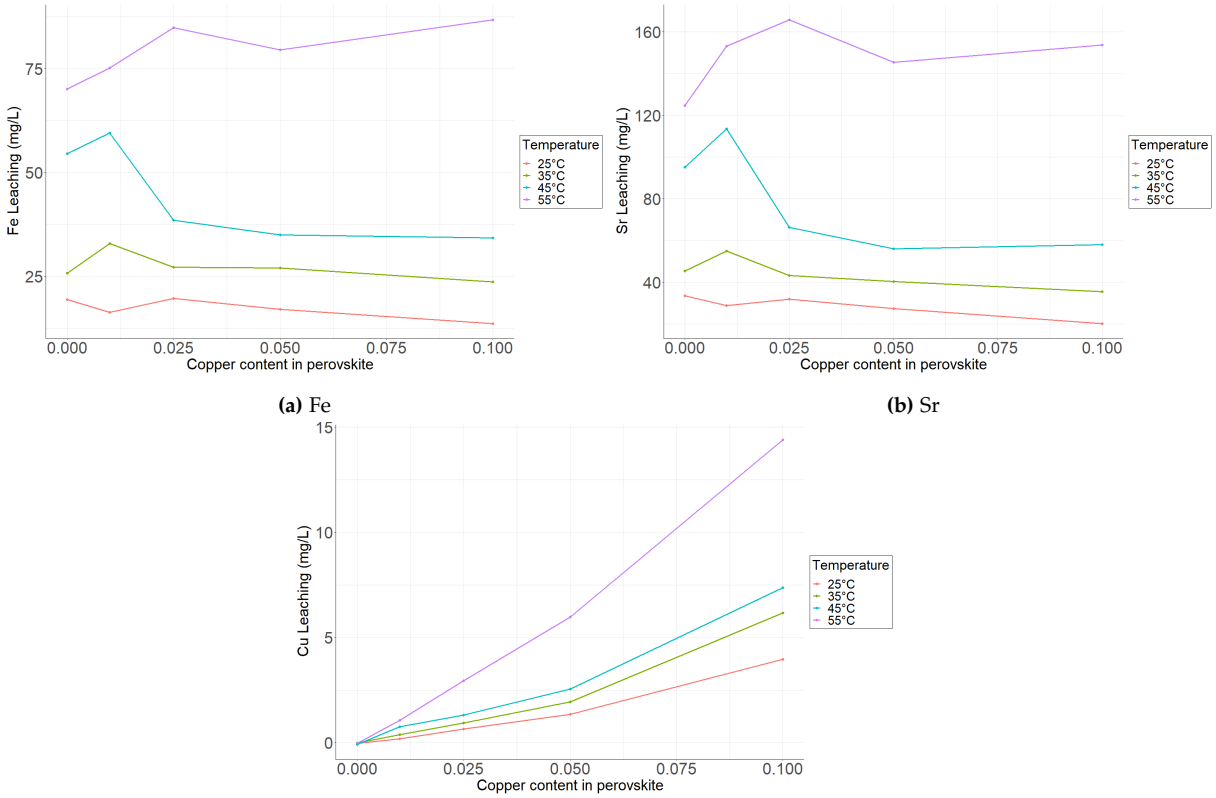


**(a)** Fe

**(b)** Sr

**(c)** Cu

**Figure 5.14:** Overview of leaching of different metals as a function of copper content

The leaching as a function of temperature can be found in **Figure E.1** showing a similar trend for the leaching of iron and strontium. In general, it can be observed that a higher temperature leads to a higher degree of leaching. This is also to be expected as the rate constant increases (**See Figure 5.7**) causing more reactions to occur and the likelihood of leaching increases. Leaching and the catalytic rates are comparable as an increase in leaching would also decrease the rate of the catalytic reaction as less catalytic material is present to operate.

The leaching of metals for the recirculation experiment can be seen from **Figure 5.15**. A clear trend can be observed as the leaching of copper and iron respectively increases and decreases as a function of copper content. This result is similar to those mentioned above and just as expected. A similar trend can be seen when comparing normal degradation with recirculation. A slight increase is observed initially with a decreasing strontium leaching at higher copper contents in the perovskite. The leaching of strontium is to an extent comparable to microstrain found through Rietveld refinement. 10% showed the least amount of leaches and the lowest microstrain, indicating that it is the most stable perovskite. The perovskite showing the highest amount of strontium leaching is 2.5% which also has the highest microstrain meaning that it is the least stable perovskite. The leaching % of each metal is calculated and can be seen in **Appendix H**. From these calculations, it is clear that the perovskite is very unstable as it leaches as much as 36.27% strontium. The leaching % for recycling is not as extensive compared to the normal thermal catalysis which can be explained as the leaching happens early. This results in the samples taken early in the cycle experiment having a high amount of leach metals causing the general leaching to decrease after 4th cycle as there are much fewer metals remaining in the perovskite to leach.

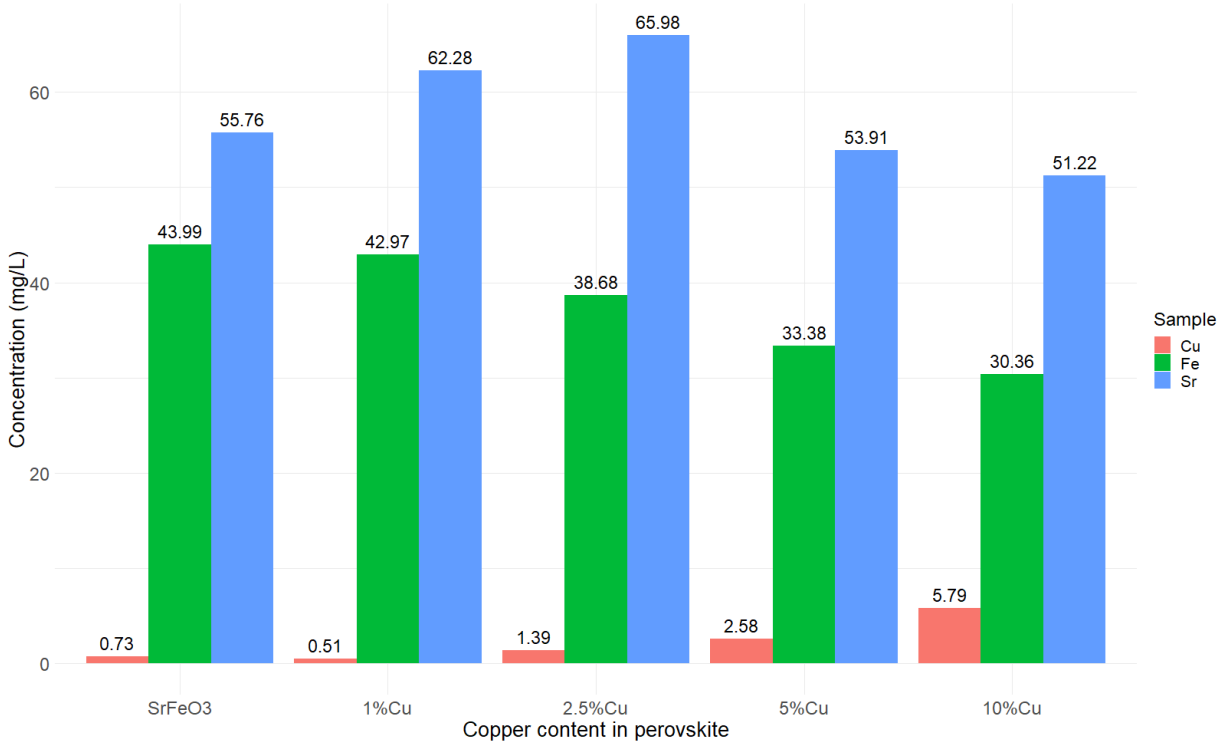


**Figure 5.15:** Illustration of the leaching of iron, copper, and strontium when recirculating the perovskites 4 times.

# Chapter 6
# Discussion

Zinc, nickel, and copper doped $SrFeO_3$ were synthesized and characterized by XRD to determine if single-phase perovskite was obtained. Unexpectedly, nickel and zinc doping saw a small peak next to the main perovskite peak indicating two phases whereas copper doped proved to be single-phased as expected. Through Rietveld refinement the comparison of the phases of $Sr_8Fe_8O_{23}$ and $Sr_4Fe_4O_{11}$ with the latter showing the best fits. This is also supported by literature also seeing the orthorhombic structure.

Through UV-Vis measurements, it was discovered that the degradation of Rh-B resulted in the disappearance of Rh-B completely following a first-order reaction. This is supported in literature by multiple sources [9, 11, 42]. From the recycling experiments, it was concluded that the ability of pure $SrFeO_3$ to treat Rh-B weakens significantly more than for copper-doped $SrFeO_3$. The rate constant of the recycling experiment showed a general decreasing trend. This is an unfortunate trend as catalysts should ideally not degrade over time since it does not interact with the overall reaction.

Another factor for a catalyst's effectiveness is its stability. In general, the perovskites showed extensive leaching of metals. This was an unfortunate but somewhat expected observation as leaching of $SrFeO_3$-based perovskites has been touched upon in literature. A reason for this may be due to the low operating pH values as literature observed less leaching at higher pH [10].
Another plausible reason for the decreased catalytic activity could be the poisoning of the perovskite during degradation. Carbonate formation in $SrFeO_3$-based perovskite is commonly seen in literature as chemisorption occurs blocking the catalytic sites of the perovskite [40]. Through XPS it was observed that the proportion of $SrCO_3$ decreases when the copper doping increases which possibly indicates that leaching is the main cause for the weakening of the catalytic effect. The XPS measurement also showed an increase in $Fe^{4+}$-ion with increased copper content which is supported by literature that saw similar trends. However, the proportion of $Fe^{4+}$-ion was significantly lower than what literature suggests which is a trend that is unable to be explained [25].

# Chapter 7
# Conclusion

In this project, the doping of the B-site of $SrFeO_3$ with nickel, zinc, and copper as dopants to see how it affects $Fe^{+4}$-ion content and the degradation of Rh-B. The degradation happened through thermal catalysis under dark ambient conditions.
The nickel-, zinc- and copper-doped $SrFeO_3$ were characterized by XRD. The measurement showed that doping of zinc and nickel would consist of more than one phase. However single phase perovskites was observed for copper doping of $SrFeO_3$ and pure $SrFeO_3$ resulting in these being the focus of this project.
The pure and copper doped $SrFeO_3$ was also characterized by XPS and the thermocatalytic properties were analyzed by determining the change in concentration of Rh-B through UV-Vis. The stability of the perovskites was analyzed by AAS by measuring the amount of leached metals occurring during thermal catalysis.
The XPS measurements showed an increase in $Fe^{+4}$ as the copper content of the perovskite increased. Additionally, the ratio of $\frac{O_L}{O_{ads}}$ indicates that the content of oxygen vacancies also increases with copper content.
Through UV-Vis measurements, it was discovered that the degradation of Rh-B resulted in the disappearance of Rh-B completely following a first-order reaction. From the recycling experiments, it was concluded that the ability of pure $SrFeO_3$ to treat Rh-B weakens significantly more than for copper-doped $SrFeO_3$. The rate constant of the recycling experiment showed a general decreasing trend. This is an unfortunate trend as catalysts should ideally not degrade over time since it does not interact with the overall reaction.
A noteworthy observation is that when degrading with copper-doped $SrFeO_3$ the liquid after the recycling experiment, would have a strong green color. This hypsochromic shift and green color are attributed to the *N*-deethylation of Rh-B into Rh-110.

The trend for the overall rate constants showed declining as the copper content increased, as 10% copper content and pure $SrFeO_3$ weakened the most during recycling. 1% copper content displayed the best rate constant over time. The weakening of the catalytic effects could be attributed to the leaching of metals over time into the solution as the leaching was excessive. An expected and clear trend was seen for the B site cations of iron and copper. Copper leaching increases as the copper content in the perovskite increases. The opposite was observed for iron leaching as it decreased with increased copper content.

The activating energy of the different copper content showed a general trend of increased copper content resulting in lower activation energy. An exception to this was observed at 10% copper displaying the highest activation energy. This is relatively in agreement with the decrease in rate constant, as a faster catalyst would result in a higher degree of catalyst poisoning.

In general, the doping of perovskite with copper suggests an increased catalytic effect. However, this increase also leads to a higher degree of leaching making it difficult for the perovskite

to maintain a continuous rate constant. The leaching of metals into the solution saw as high percentages as 36.27%, making it a plausible cause for the decreasing catalytic effect.

# Chapter 8
# Further research

An interesting further investigation would be that of another organic pollutant instead of using a dye. This could for example be a more relevant organic pollutant such as diclofenac, a medication for pain management, as commonly seen in polluting aquatic environments. Diclofenac is known to be toxic, even at deficient concentrations ($\frac{ng}{L}$), and is, therefore, a relevant organic pollutant to analyze [46].

Changing the pH of the thermal catalysis could also be an interesting aspect to further analyze. Palma et al. used cerium doped $SrFeO_3$ for thermal catalysis at different pH levels. They found the leaching of metals to be significantly larger at lower pH and saw little to no leaching at higher pH values. A similar trend might occur even though a different dopant and organic pollutant is used [10].

As mentioned in **Section 5.1** zinc and nickel doped $SrFeO_3$ did not provide a clean single-phased perovskite. It is therefore interesting to see if altering the synthesis parameters such as pH, fuel-to-metal cation ratio, reducer-to-oxidizer ratio, and/or fuel type would form single-phase perovskite. Nickel and zinc are interesting because, like copper, their most abundant oxidation state is +2 which would in theory create more $Fe^{4+}$-ions.
Yang et al. doped $SrFeO_3$ with nickel successfully through the sol-gel method which is somewhat to that of the solution combustion synthesis [47]. It could therefore be interesting to go that route when doping with nickel.

After every experiment, the remaining perovskites were saved in hopes of performing XRD to determine possible carbonate formation during the degradation of Rh-B. However, not enough perovskites were left to get tightly packed XRD samples. Increasing the amount of perovskite in the degradation experiment could therefore be done in further work as it would be interesting to do XRD tests but also see the effect of degradation when varying the concentration of perovskite. Another way of testing for possible carbonate formation could be by FT-IR.

Possible further research could be doing the recirculation experiments at 25°C, 35°C, and 55°C as well to how the degradation is impacted when some of the Rh-B is still present when recirculation occurs.

# Bibliography


[1] Huihuang Chen, Jiangang Ku, and Lianzhou Wang. "Thermal catalysis under dark ambient conditions in environmental remediation: Fundamental principles, development, and challenges". eng. In: *Chinese journal of catalysis* 40.8 (2019), pp. 1117–1134. ISSN: 1872-2067.

[2] Kaj Sand Jensen and Claus Lindegaard. *Forurening med miljøfremmede stoffer*. NATUREN I DANMARK. 2014. URL: https://naturenidanmark.lex.dk/Forurening_med_milj%C3%B8fremmede_stoffer.

[3] Muhammad Farhan Hanafi and Norzahir Sapawe. "A review on the current techniques and technologies of organic pollutants removal from water/wastewater". eng. In: *Materials Today: Proceedings* 31 (2020), A158–A165. ISSN: 2214-7853.

[4] Arpita Roy et al. "Phytogenic Synthesis of Metal/Metal Oxide Nanoparticles for Degradation of Dyes". eng. In: *Journal of renewable materials* 10.7 (2022), pp. 1911–1930. ISSN: 2164-6325.

[5] LibreTexts Chemistry. The royal society of chemistry. 2015. URL: https://www.rsc.org/suppdata/ra/c4/c4ra14184a/c4ra14184a1.pdf.

[6] Jyotshana Sharma et al. "Toxic effects of Rhodamine B on antioxidant system and photosynthesis of Hydrilla verticillata". eng. In: *Journal of hazardous materials letters* 3 (2022), pp. 100069–. ISSN: 2666-9110.

[7] Perovskite-info. *An introduction to Perovskites*. Perovskite-info. 2024. URL: https://www.perovskite-info.com/introduction.

[8] Bradley Wilson. *What are perovskites and their applications*. The Glasgow insight into science and technology. 2020. URL: https://the-gist.org/2020/01/perovskites-best-material-youve-never-heard-of/.

[9] Martin Bonderup Østergaard et al. "Kinetics of Strontium Carbonate Formation on a Ce-Doped SrFeO3 Perovskite". eng. In: (2022). ISSN: 20734344.

[10] Davide Palma et al. "Main Issues in the Synthesis and Testing of Thermocatalytic Ce-Doped SrFeO3 Perovskites for Wastewater Pollutant Removal". eng. In: (2023). ISSN: 23046740.

[11] Maria Laura Tummino et al. "Revisiting the catalytic activity of a doped SrFeO3 for water pollutants removal: Effect of light and temperature". eng. In: *Applied catalysis. B, Environmental* 207 (2017), pp. 174–181. ISSN: 0926-3373.

[12] Jian Dou et al. "A- and B-site Codoped SrFeO3 Oxygen Sorbents for Enhanced Chemical Looping Air Separation". eng. In: *ChemSusChem* 13.2 (2020), pp. 385–393. ISSN: 1864-5631.

[13] Kai Wang et al. "Perovskite Oxide Catalysts for Advanced Oxidation Reactions". eng. In: *Advanced functional materials* 31.30 (2021). ISSN: 1616-301X.

[14] Maria Laura Tummino. *Current research in green and sustainable chemistry (Online)*. eng. Amsterdam, 2020.

[15] Dr. Mary O'Kane. "Perovskite Solar Cells: Methods of Increasing Stability and Durability". In: *Chinese journal of catalysis* (2019).

[16] Stuart Thomson. "Observing Phase Transitions in a Halide Perovskite Using Temperature Dependent Photoluminescence Spectroscopy". In: (May 2018).

[17] Mohammed Ismael and Michael Wark. "Perovskite-type LaFeO3: Photoelectrochemical properties and photocatalytic degradation of organic pollutants under visible light irradiation". eng. In: *Catalysts* 9.4 (2019), pp. 342–. ISSN: 2073-4344.

[18] Shabina Kappadan et al. "Tetragonal BaTiO3 nanoparticles: An efficient photocatalyst for the degradation of organic pollutants". eng. In: *Materials science in semiconductor processing* 51 (2016), pp. 42–47. ISSN: 1369-8001.

[19] Wei Zhong et al. "Mechanism studies on methyl orange dye degradation by perovskite-type LaNiO3-δ under dark ambient conditions". eng. In: *Applied catalysis. A, General* 549.C (2018), pp. 302–309. ISSN: 0926-860X.

[20] Jonathan Hwang et al. "Perovskites in catalysis and electrocatalysis". eng. In: *Science (American Association for the Advancement of Science)* 358.6364 (2017), pp. 751–757. ISSN: 0036-8075.

[21] Xue Li et al. "A-site perovskite oxides: an emerging functional material for electrocatalysis and photocatalysis". eng. In: *Journal of materials chemistry. A, Materials for energy and sustainability* 9.11 (2021), pp. 665–667. ISSN: 2050-7488.

[22] Prof. Robin Grimes. *Database of Ionic Radii*. Atomistic Simulation Group. URL: `http://abulafia.mt.ic.ac.uk/shannon/ptable.php`.

[23] F. Deganello et al. "Cerium effect on the phase structure, phase stability and redox properties of Ce-doped strontium ferrates". eng. In: *Journal of solid state chemistry* 179.11 (2006), pp. 3406–3419. ISSN: 0022-4596.

[24] Qiang Sun et al. "Insights into the oxygen reduction reaction on Cu-doped SrFeO3-δ cathode for solid oxide fuel cells". eng. In: *Journal of power sources* 497 (2021). ISSN: 0378-7753.

[25] Qiang Sun et al. "Insights into the oxygen reduction reaction on Cu-doped SrFeO3-δ cathode for solid oxide fuel cells". eng. In: *Journal of power sources* 497 (2021). ISSN: 0378-7753.

[26] Francesca Deganello and Avesh Kumar Tyagi. "Solution combustion synthesis, energy and environment: Best parameters for better materials". eng. In: *Progress in crystal growth and characterization of materials* 64.2 (2018), pp. 23–61. ISSN: 0960-8974.

[27] Emanuel Carlos et al. "Solution Combustion Synthesis: Towards a Sustainable Approach for Metal Oxides". eng. In: *Chemistry : a European journal* 26.42 (2020), pp. 9099–9125. ISSN: 0947-6539.

[28] F. Deganello, G. Marcì, and G. Deganello. "Citrate–nitrate auto-combustion synthesis of perovskite-type nanopowders: A systematic approach". eng. In: *Journal of the European Ceramic Society* 29.3 (2009), pp. 439–450. ISSN: 0955-2219.

[29] Hyu-Bum Park et al. "Preparation of La1-xSrxMnO3 powders by combustion of poly(ethylene glycol)-metal nitrate gel precursors". eng. In: *Journal of materials science* 32.1 (1997), pp. 57–65. ISSN: 0022-2461.

[30] C. Cannas et al. “CoFe2O4 nanocrystalline powders prepared by citrate-gel methods: Synthesis, structure and magnetic properties”. eng. In: *Journal of nanoparticle research : an interdisciplinary forum for nanoscale science and technology* 8.2 (2006), pp. 255–267. ISSN: 1388-0764.

[31] Barbara Kucharczyk et al. “The effect of the calcination temperature of LaFeO3 precursors on the properties and catalytic activity of perovskite in methane oxidation”. eng. In: *Ceramics international* 45.2 (2019), pp. 2779–2788. ISSN: 0272-8842.

[32] Akula Naveenkumar et al. “Mixture of Fuels Approach for the Synthesis of SrFeO3δ Nanocatalyst and Its Impact on the Catalytic Reduction of Nitrobenzene”. eng. In: *Inorganic chemistry* 53.22 (2014), pp. 12178–12185. ISSN: 0020-1669.

[33] Junjiang Zhu et al. “Perovskite Oxides: Preparation, Characterizations, and Applications in Heterogeneous Catalysis”. eng. In: *ACS catalysis* 4.9 (2014), pp. 2917–2940. ISSN: 2155-5435.

[34] Hamed Derikvand, Nemat Tahmasebi, and Shahram Barzegar. “Photocatalytic degradation of organic pollutants under visible light using lead-free all-inorganic halide perovskites A3Bi2Cl9 (A = Cs, Rb)”. eng. In: *The Journal of physics and chemistry of solids* 181 (2023), pp. 111528–. ISSN: 0022-3697.

[35] Shui-Wen Chang Chien et al. “Investigating the effects of various synthesis routes on morphological, optical, photoelectrochemical and photocatalytic properties of single-phase perovskite BiFeO3”. eng. In: *The Journal of physics and chemistry of solids* 160 (2022), pp. 110342–. ISSN: 0022-3697.

[36] Shenggang Li and David A Dixon. *Mechanism of oxide-catalyzed selective oxidation: A computational perspective*. Vol. 15. Annual Reports in Computational Chemistry. Elsevier, 2019. Chap. 8. ISBN: 9780128171196.

[37] Ulrich Neuenschwander and Ive Hermans. “Thermal and catalytic formation of radicals during autoxidation”. eng. In: *Journal of catalysis* 287 (2012), pp. 1–4. ISSN: 0021-9517.

[38] Abdul Majid et al. “The effect of preparation method and calcination temperature on the crystallite size and surface area of perovskite-type SrFeO x”. eng. In: *Journal of sol-gel science and technology* 32.1-3 (2004), pp. 323–326. ISSN: 0928-0707.

[39] A. Sendil Kumar et al. “Magnetism and Charge Order in Nanocrystalline Orthorhombic SrFeO3-δ”. eng. In: *Journal of superconductivity and novel magnetism* 33.6 (2020), pp. 1839–1844. ISSN: 1557-1939.

[40] Martin B. Østergaard et al. “Beneficial effect of cerium excess on in situ grown Sr0.86Ce0.14FeO3-CeO2 thermocatalysts for the degradation of bisphenol A”. eng. In: *RSC advances* 13.31 (2023), pp. 21459–21470. ISSN: 2046-2069.

[41] LibreTexts Chemistry. *Effects of Temperature, Concentration, and Catalysts on Reaction Rates*. LibreTexts Chemistry. URL: https://chem.libretexts.org/Courses/Chabot_College/Introduction_to_General_Organic_and_Biochemistry/10%3A_Reaction_Rates_and_Equilibrium/10.03%3A_Effects_of_Temperature_Concentration_and_Catalysts_on_Reaction_Rates.

[42] Chilukoti Srilakshmi, Rohit Saraf, and Chikkadasappa Shivakumara. “Effective Degradation of Aqueous Nitrobenzene Using the SrFeO3δ Photocatalyst under UV Illumination and Its Kinetics and Mechanistic Studies”. eng. In: *Industrial and engineering chemistry research* 54.32 (2015), pp. 7800–7810. ISSN: 0888-5885.

[43] Anna Jakimińska, Miłosz Pawlicki, and Wojciech Macyk. “Photocatalytic transformation of Rhodamine B to Rhodamine-110 – The mechanism revisited”. eng. In: *Journal of photochemistry and photobiology. A, Chemistry.* 433 (2022), pp. 114176–. ISSN: 1010-6030.

[44] Kaja Spilarewicz-Stanek et al. “Understanding the role of silver nanostructures and graphene oxide applied as surface modification of TiO2 in photocatalytic transformations of rhodamine B under UV and vis irradiation”. eng. In: *Materials* 13.20 (2020), pp. 1–21. ISSN: 1996-1944.

[45] Zhong He et al. “Photocatalytic degradation of rhodamine B by Bi2WO6 with electron accepting agent under microwave irradiation: Mechanism and pathway”. eng. In: *Journal of hazardous materials* 162.2-3 (2009), pp. 1477–1486. ISSN: 0304-3894.

[46] Palanivel Sathishkumar et al. “Occurrence, interactive effects and ecological risk of diclofenac in environmental compartments and biota - a review”. eng. In: *The Science of the total environment* 698 (2020), pp. 134057–134057. ISSN: 0048-9697.

[47] Liuqing Yang et al. “Effect of Nickel and Cobalt Doping on the Redox Performance of SrFeO3δ toward Chemical Looping Dry Reforming of Methane”. eng. In: *Energy fuels* 37.16 (2023), pp. 12045–12057. ISSN: 0887-0624.

[48] Samian Samian, A.H. Zaidan, and Moh Yasin. “Detection of Rhodamine B levels in distilled water based on displacement sensor using fiber coupler and concave mirror”. eng. In: *Journal of Optoelectronics and Advanced Materials* 18.11-12 (2016), pp. 988–992. ISSN: 1454-4164.

[49] Benjamin H. Christensen et al. “Thermocatalytic Performance of LaCo1xNixO3δ Perovskites in the Degradation of Rhodamine B”. eng. In: *Catalysts* 13.2 (2023), pp. 325–. ISSN: 2073-4344.

# Appendix A
# Standard Curve

To determine the the concentration from UV-spectroscopy a standard curve is made for Rh-B. On the **Figure A.1** the full spectrum of Rh-B with the concentration of 10 $\frac{mg}{L}$ and a pH of 2 is shown. The arrow shows the chosen wavelength of 555 nm due to it being the characteristic peak.

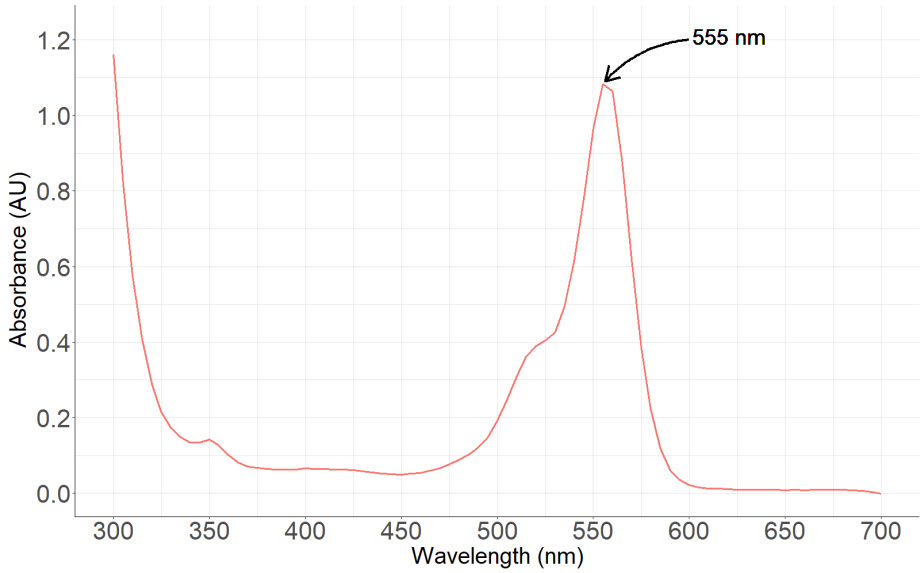


**Figure A.1:** Full spectrum of Rh-B to determine what wavelength showed the highest absorbance.

Based on this given wavelength a standard curve can now be made and fitted to linear regression. The standard curve of Rh-B ranging from 0-5 $\frac{mg}{L}$ can be seen on **Figure A.2**. It can be seen that an $R^2$-value of 0.999 is obtained which indicates a reliable standard curve.

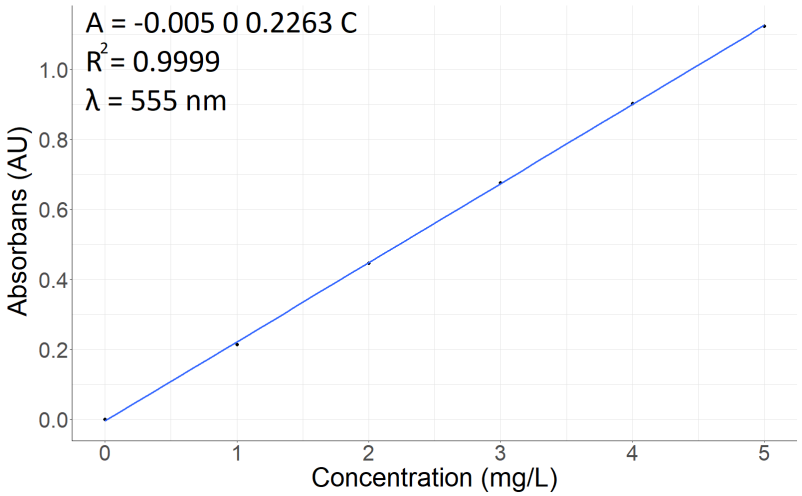


**Figure A.2:** The figure shows the standard curve for Rh-B ranging from 0-5 $\frac{mg}{L}$

To find the concentration of Rh-B over time the Beer-Lambert law (absorption equation) is used and can be seen below in **Equation A.1**:

$$A = \epsilon \cdot C \cdot L \tag{A.1}$$

where A is the absorbance found in UV-vis measurements, $\epsilon$ is the so-called extinction coefficient, C is the concentration of Rh-B in the solution at a given time and L is the path length of the light through the sample. Results can be seen in **Table A.1**.

**Table A.1:** Values obtained from standard curve

| Molecule | Absorption equation $\left(C\left[\frac{\text{mg}}{\text{L}}\right]\right)$ | $R^2$ | wavelength (nm) | $\varepsilon$ $(\frac{\text{L}}{\text{mg}\cdot\text{cm}})$ | wavelength found from literature (nm) |
|---|---|---|---|---|---|
| Rhodamine B | A = -0.005 + 0.2263 · C | 0.9999 | 555 | 0.2263 | 553.5 [48] - 558 [49] |

# Appendix B
# Measured materials

General overview of all measured materials for synthesis. All values are in gram except pH.

| | Cu0 | Cu1 | Cu2.5 | Cu5 | Cu10 |
|---|---|---|---|---|---|
| $Sr(NO_3)_2$ | 2.1152 | 2.1163 | 2.116 | 2.1168 | 2.1159 |
| $Fe(NO_3)_2 \cdot 9H_2O$ | 4.04 | 3.9997 | 3.9388 | 3.8384 | 3.6362 |
| $Cu(NO_3)_2 \cdot 3H_2O$ | 0 | 0.0239 | 0.061 | 0.1204 | 0.2417 |
| Citric acid | 7.6849 | 7.6856 | 7.6847 | 7.6844 | 7.6851 |
| $NH_4NO_3$ | 9.2054 | 9.2246 | 9.2551 | 9.3043 | 9.4944 |
| pH | 3.15 | 3.143 | 3.152 | 3.147 | 3.141 |

**Table B.1:** 1st Synthesis of copper doped $SrFeO_3$

| | Cu0 | Cu1 | Cu2.5 | Cu5 | Cu10 |
|---|---|---|---|---|---|
| $Sr(NO_3)_2$ | 2.1168 | 2.1158 | 2.1156 | 2.1163 | 2.1158 |
| $Fe(NO_3)_2 \cdot 9H_2O$ | 4.0394 | 3.9995 | 3.9388 | 3.8385 | 3.6359 |
| $Cu(NO_3)_2 \cdot 3H_2O$ | 0 | 0.0242 | 0.0617 | 0.1215 | 0.2419 |
| Citric acid | 7.6826 | 7.6842 | 7.6848 | 7.6853 | 7.6844 |
| $NH_4NO_3$ | 9.2025 | 9.2248 | 9.2541 | 9.3043 | 9.4945 |
| pH | 3.138 | 3.136 | 3.145 | 3.14 | 3.137 |

**Table B.2:** 2nd Synthesis of copper doped $SrFeO_3$

| | Cu0 | Cu1 | Cu2.5 | Cu5 | Cu10 |
|---|---|---|---|---|---|
| $Sr(NO_3)_2$ | 2.1165 | 2.1162 | 2.1159 | 2.1158 | 2.1165 |
| $Fe(NO_3)_2 \cdot 9H_2O$ | 4.0412 | 3.9995 | 3.9384 | 3.8385 | 3.6362 |
| $Cu(NO_3)_2 \cdot 3H_2O$ | 0 | 0.0245 | 0.0607 | 0.1206 | 0.2415 |
| Citric acid | 7.6836 | 7.6855 | 7.6852 | 7.6854 | 7.6848 |
| $NH_4NO_3$ | 9.2052 | 9.2245 | 9.255 | 9.3051 | 9.4949 |
| pH | 3.134 | 3.147 | 3.155 | 3.15 | 3.144 |

**Table B.3:** 3rd Synthesis of copper doped $SrFeO_3$

| | Zn0 | Zn1 | Zn2.5 | Zn5 | Zn10 |
|---|---|---|---|---|---|
| $Sr(NO_3)_2$ | 2.1152 | 2.1159 | 2.1164 | 2.1166 | 2.1159 |
| $Fe(NO_3)_2 \cdot 9H_2O$ | 4.04 | 4.0006 | 3.9383 | 3.8387 | 3.6361 |
| $Zn(NO_3)_2 \cdot 6H_2O$ | 0 | 0.0295 | 0.0747 | 0.1496 | 0.2984 |
| Citric acid | 7.6849 | 7.6852 | 7.6855 | 7.6842 | 7.6852 |
| $NH_4NO_3$ | 9.2054 | 9.2249 | 9.2548 | 9.3051 | 9.4045 |
| pH | 3.15 | 3.147 | 3.142 | 3.138 | 3.137 |

**Table B.4:** 1st Synthesis of zinc doped $SrFeO_3$

| | Zn0 | Zn1 | Zn2.5 | Zn5 | Zn10 |
|---|---|---|---|---|---|
| $Sr(NO_3)_2$ | 2.1168 | 2.1159 | 2.1165 | 2.1169 | 2.1167 |
| $Fe(NO_3)_2 \cdot 9H_2O$ | 4.0394 | 4.0005 | 3.9384 | 3.837 | 3.6368 |
| $Zn(NO_3)_2 \cdot 6H_2O$ | 0 | 0.0306 | 0.0747 | 0.1477 | 0.2973 |
| Citric acid | 7.6826 | 7.6853 | 7.6842 | 7.6852 | 7.6847 |
| $NH_4NO_3$ | 9.2025 | 9.2249 | 9.2548 | 9.3045 | 9.4054 |
| pH | 3.138 | 3.139 | 3.135 | 3.137 | 3.134 |

**Table B.5:** 2nd Synthesis of zinc doped $SrFeO_3$

| | Zn0 | Zn1 | Zn2.5 | Zn5 | Zn10 |
|---|---|---|---|---|---|
| $Sr(NO_3)_2$ | 2.1165 | 2.1159 | 2.1164 | 2.1166 | 2.1167 |
| $Fe(NO_3)_2 \cdot 9H_2O$ | 4.0412 | 4.0009 | 3.9395 | 3.8371 | 3.6368 |
| $Zn(NO_3)_2 \cdot 6H_2O$ | 0 | 0.0308 | 0.075 | 0.148 | 0.2984 |
| Citric acid | 7.6836 | 7.6853 | 7.6851 | 7.6851 | 7.6852 |
| $NH_4NO_3$ | 9.2052 | 9.2243 | 9.2553 | 9.3042 | 9.4048 |
| pH | 3.134 | 3.145 | 3.157 | 3.14 | 3.134 |

**Table B.6:** 3rd Synthesis of zinc doped $SrFeO_3$

| | Ni0 | Ni1 | Ni2.5 | Ni5 | Ni10 |
|---|---|---|---|---|---|
| $Sr(NO_3)_2$ | 2.1152 | 2.116 | 2.1164 | 2.1162 | 2.1163 |
| $Fe(NO_3)_2 \cdot 9H_2O$ | 4.04 | 4.0001 | 3.9395 | 3.8371 | 3.6368 |
| $Ni(NO_3)_2 \cdot 6H_2O$ | 0 | 0.0212 | 0.0521 | 0.1053 | 0.2092 |
| Citric acid | 7.6849 | 7.685 | 7.6855 | 7.6855 | 7.6849 |
| $NH_4NO_3$ | 9.2054 | 9.2256 | 9.2549 | 9.305 | 9.4052 |
| pH | 3.15 | 3.151 | 3.138 | 3.144 | 3.149 |

**Table B.7:** 1st Synthesis of nickel doped $SrFeO_3$

| | Ni0 | Ni1 | Ni2.5 | Ni5 | Ni10 |
|---|---|---|---|---|---|
| $Sr(NO_3)_2$ | 2.1168 | 2.1164 | 2.1161 | 2.1168 | 2.1169 |
| $Fe(NO_3)_2 \cdot 9H_2O$ | 4.0394 | 4.0001 | 3.9388 | 3.8381 | 3.6363 |
| $Ni(NO_3)_2 \cdot 6H_2O$ | 0 | 0.0206 | 0.0528 | 0.1049 | 0.2093 |
| Citric acid | 7.6826 | 7.6854 | 7.6848 | 7.6853 | 7.6855 |
| $NH_4NO_3$ | 9.2025 | 9.2251 | 9.2551 | 9.3049 | 9.405 |
| pH | 3.138 | 3.152 | 3.137 | 3.141 | 3.145 |

**Table B.8:** 2nd Synthesis of nickel doped $SrFeO_3$

| | Ni0 | Ni1 | Ni2.5 | Ni5 | Ni10 |
|---|---|---|---|---|---|
| $Sr(NO_3)_2$ | 2.1165 | 2.1165 | 2.1162 | 2.1164 | 2.1155 |
| $Fe(NO_3)_2 \cdot 9H_2O$ | 4.0412 | 3.9997 | 3.9392 | 3.8386 | 3.6363 |
| $Ni(NO_3)_2 \cdot 6H_2O$ | 0 | 0.0202 | 0.0515 | 0.1051 | 0.2099 |
| Citric acid | 7.6836 | 7.6857 | 7.6855 | 7.6848 | 7.6855 |
| $NH_4NO_3$ | 9.2052 | 9.2252 | 9.2555 | 9.3043 | 9.4048 |
| pH | 3.134 | 3.143 | 3.137 | 3.135 | 3.16 |

**Table B.9:** 3rd Synthesis of nickel doped $SrFeO_3$

# Appendix C
# Degradation

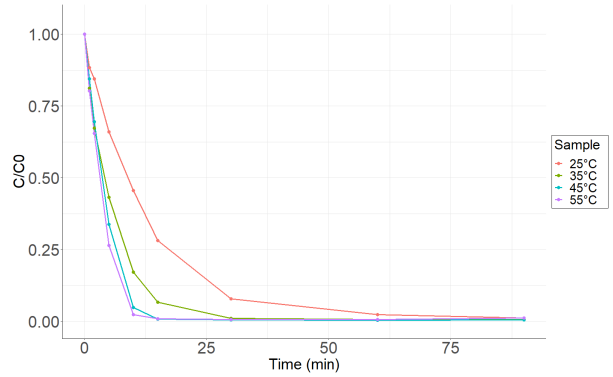


**(a)** Degradation with 1% copper content

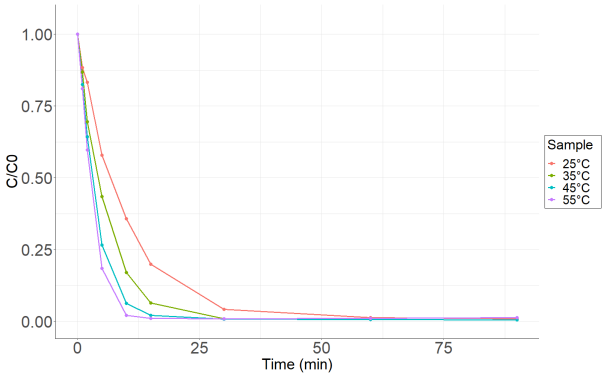


**(b)** Degradation with 2.5% copper content

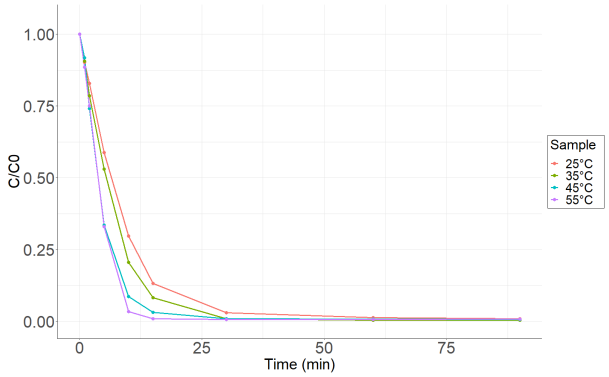


**(c)** Degradation with 5% copper content

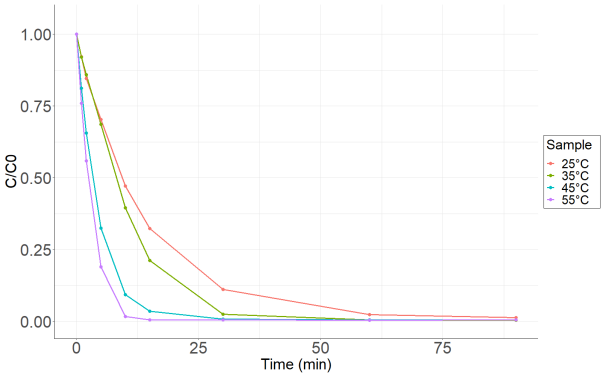


**(d)** Degradation with 10% copper content

**Figure C.1:** The figures illustrate degradation with at different temperatures for each synthesized perovskite.

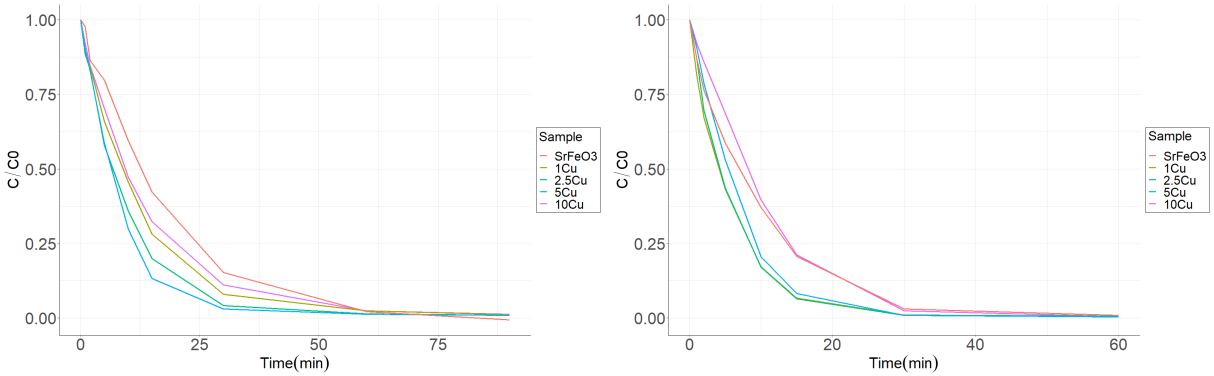


**(a)** Degradation at 25 °C




**(b)** Degradation at 45 °C

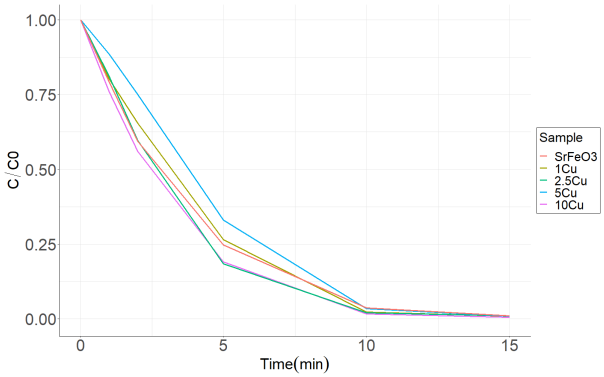


**(c)** Degradation at 55 °C

**Figure C.2:** Degradation at different temperatures.

# Appendix D
# Rate constant

| Perovskite | Temperature (°C) | Rate constant ($\frac{1}{s}$) | $R^2$ |
|---|---|---|---|
| $SrFeO_3$ | 25 | $1.07 \cdot 10^{-3}$ | 0.999 |
| $SrFeO_3$ | 35 | $1.37 \cdot 10^{-3}$ | 0.953 |
| $SrFeO_3$ | 45 | $2.96 \cdot 10^{-3}$ | 0.990 |
| $SrFeO_3$ | 55 | $5.25 \cdot 10^{-3}$ | 0.996 |
| 1%Cu | 25 | $8.7 \cdot 10^{-4}$ | 0.953 |
| 1%Cu | 35 | $2.54 \cdot 10^{-3}$ | 0.990 |
| 1%Cu | 45 | $3.22 \cdot 10^{-3}$ | 0.862 |
| 1%Cu | 55 | $5.54 \cdot 10^{-3}$ | 0.979 |
| 2.5%Cu | 25 | $1.72 \cdot 10^{-4}$ | 0.909 |
| 2.5%Cu | 35 | $2.61 \cdot 10^{-3}$ | 0.999 |
| 2.5%Cu | 45 | $2.85 \cdot 10^{-3}$ | 0.905 |
| 2.5%Cu | 55 | $5.42 \cdot 10^{-3}$ | 0.971 |
| 5%Cu | 25 | $9.2 \cdot 10^{-4}$ | 0.860 |
| 5%Cu | 35 | $2.67 \cdot 10^{-3}$ | 0.895 |
| 5%Cu | 45 | $2.77 \cdot 10^{-3}$ | 0.933 |
| 5%Cu | 55 | $5.54 \cdot 10^{-3}$ | 0.987 |
| 10%Cu | 25 | $8.5 \cdot 10^{-4}$ | 0.965 |
| 10%Cu | 35 | $1.54 \cdot 10^{-3}$ | 0.964 |
| 10%Cu | 45 | $2.79 \cdot 10^{-3}$ | 0.958 |
| 10%Cu | 55 | $6.03 \cdot 10^{-3}$ | 0.986 |

**Table D.1:** overview of all rate constants

# Appendix E
# Leaching of metals

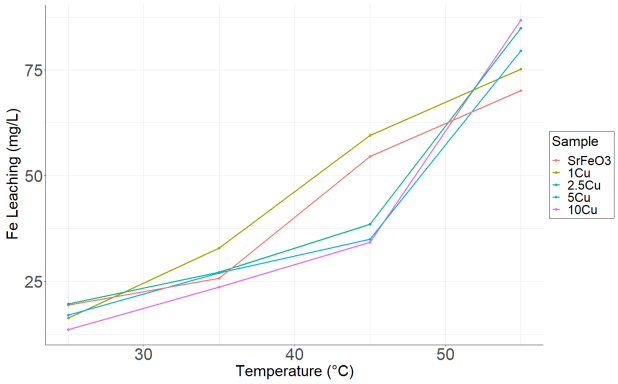


**(a)** Iron leaching as a function of temperature.

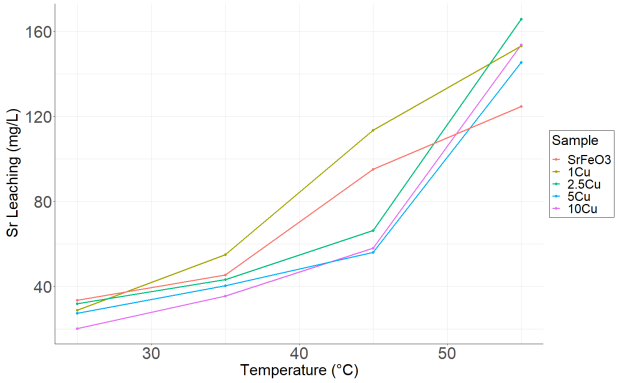


**(b)** Strontium leaching as a function of temperature.

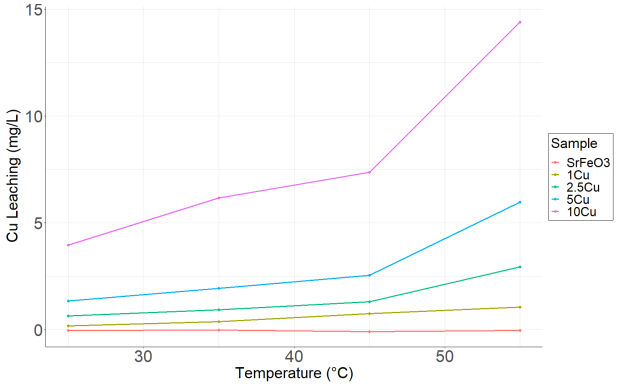


**(c)** Copper leaching as a function of temperature.

**Figure E.1:** Leaching of iron, strontium, and copper as a function of temperature.

# Appendix F
# Solution post-recycling

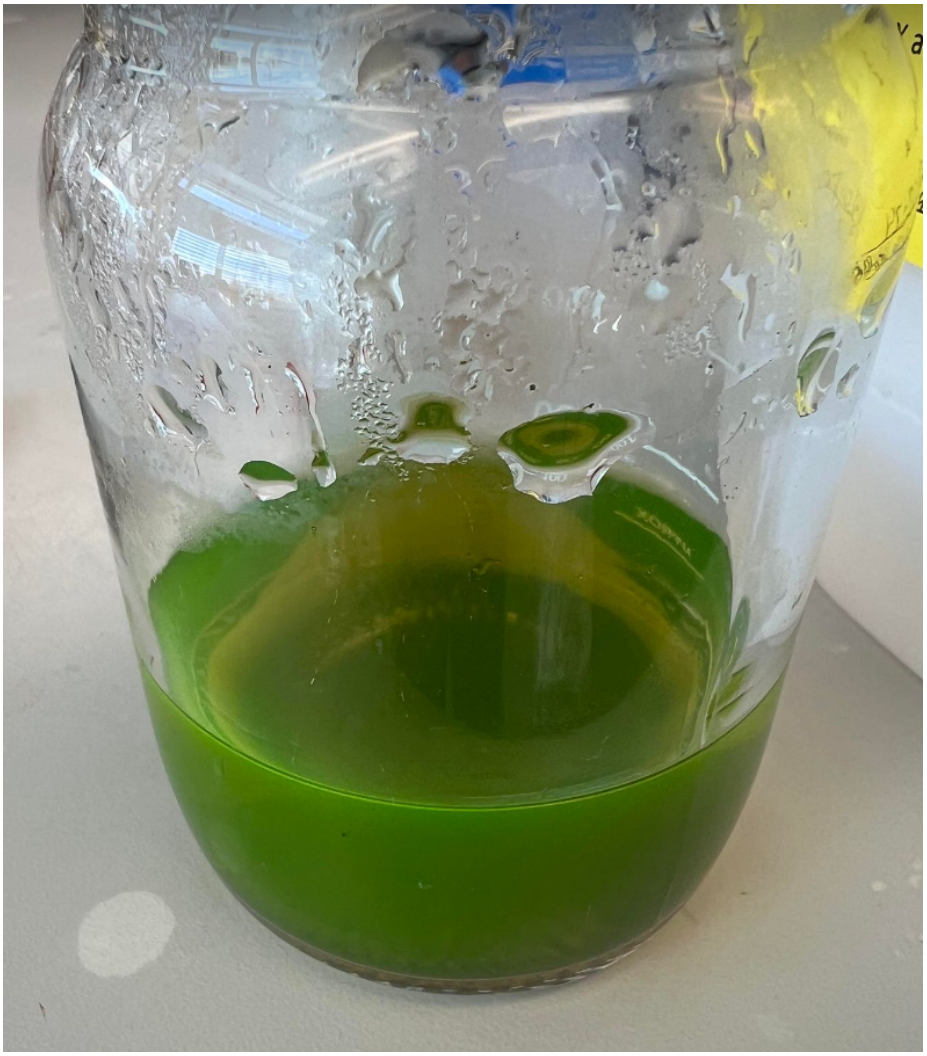

**Figure F.1:** The solution after using 5% copper content for recycling experiment.

# Appendix G
# Recirculation

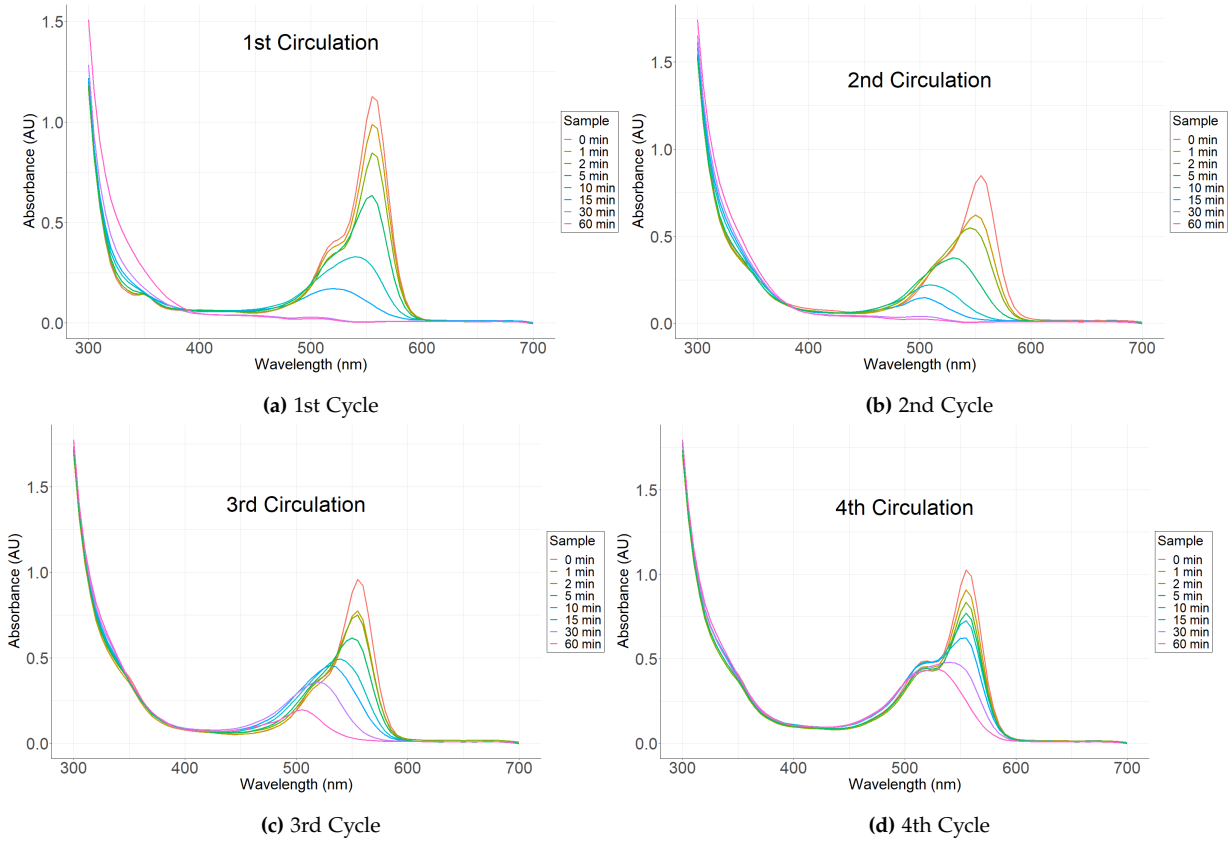


**(a)** 1st Cycle

**(b)** 2nd Cycle

**(c)** 3rd Cycle

**(d)** 4th Cycle

**Figure G.1:** Cycles for $SrFeO_3$

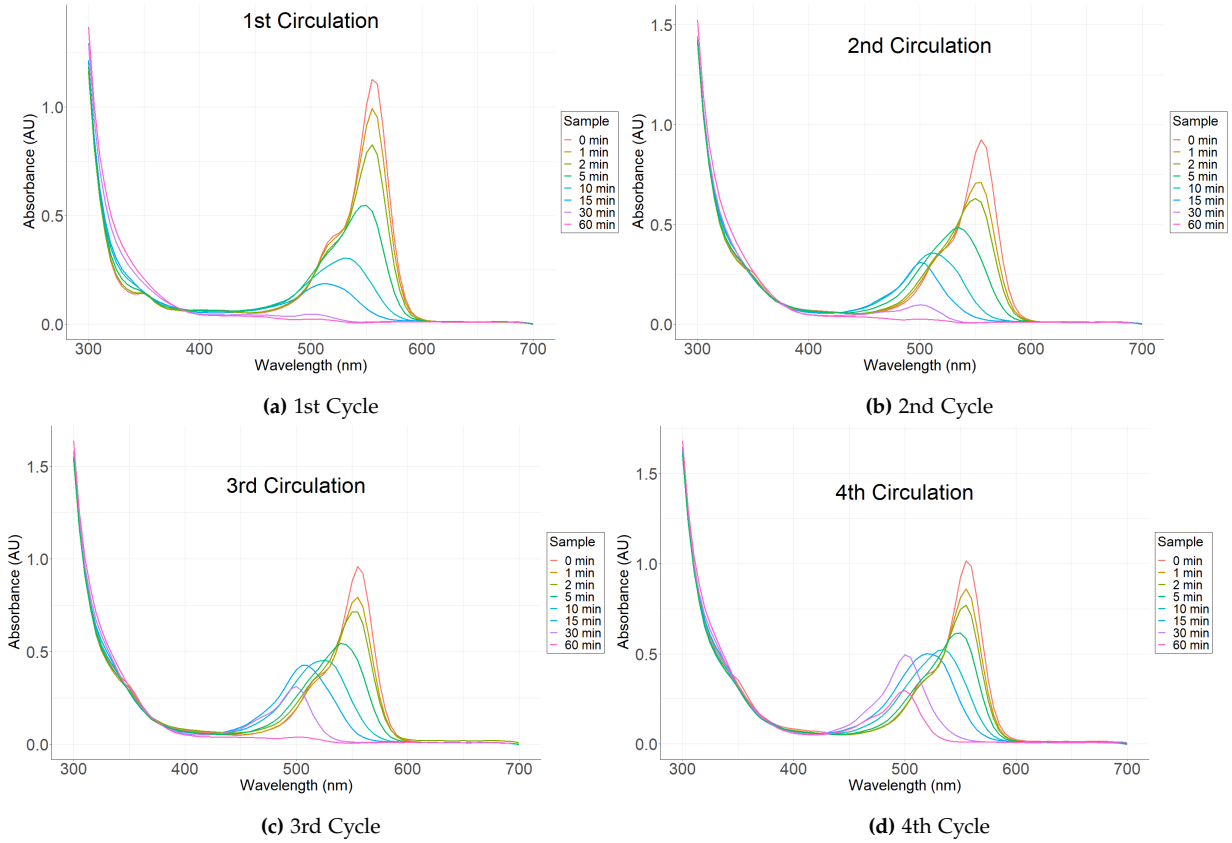


**(a)** 1st Cycle

**(b)** 2nd Cycle

**(c)** 3rd Cycle

**(d)** 4th Cycle

**Figure G.2:** Cycles for 1%Cu-doped $SrFeO_3$

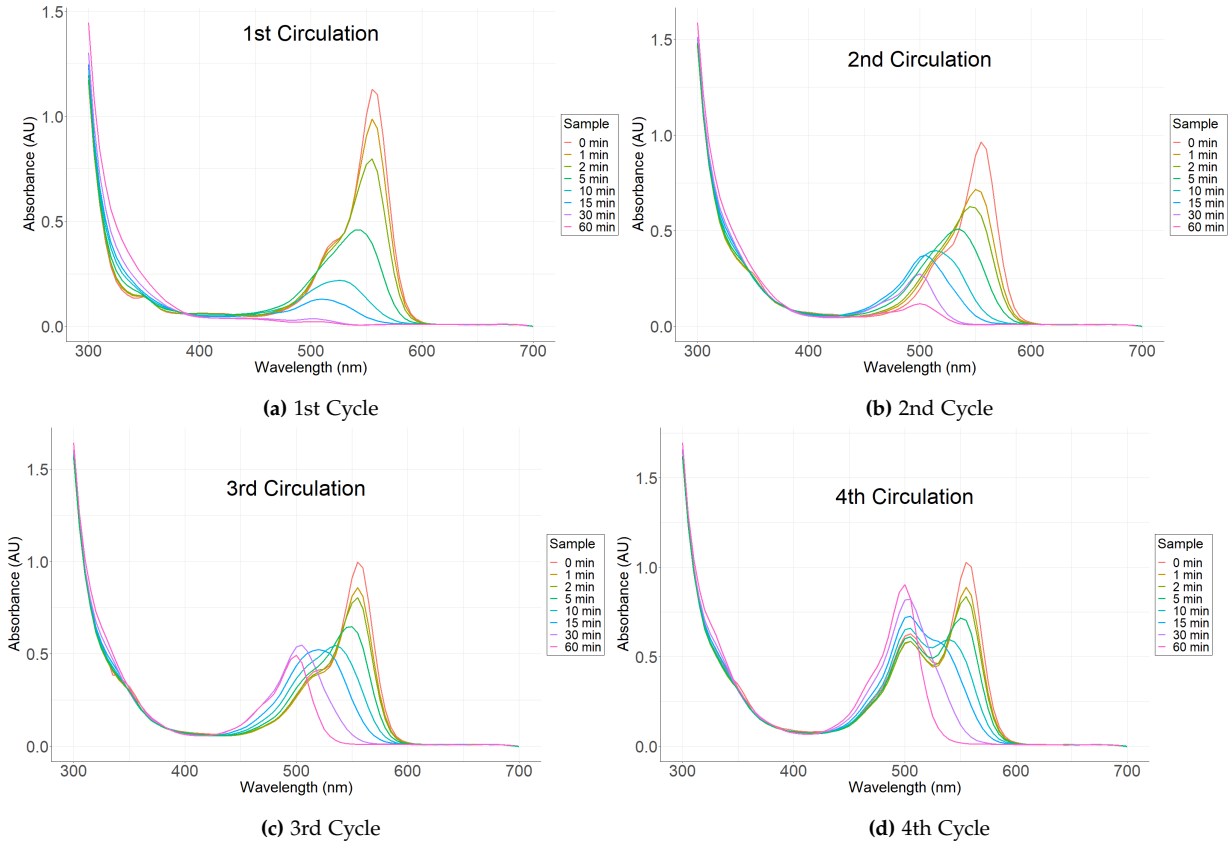


**(a)** 1st Cycle

**(b)** 2nd Cycle

**(c)** 3rd Cycle

**(d)** 4th Cycle

**Figure G.3:** Cycles for 2.5%Cu-doped $SrFeO_3$

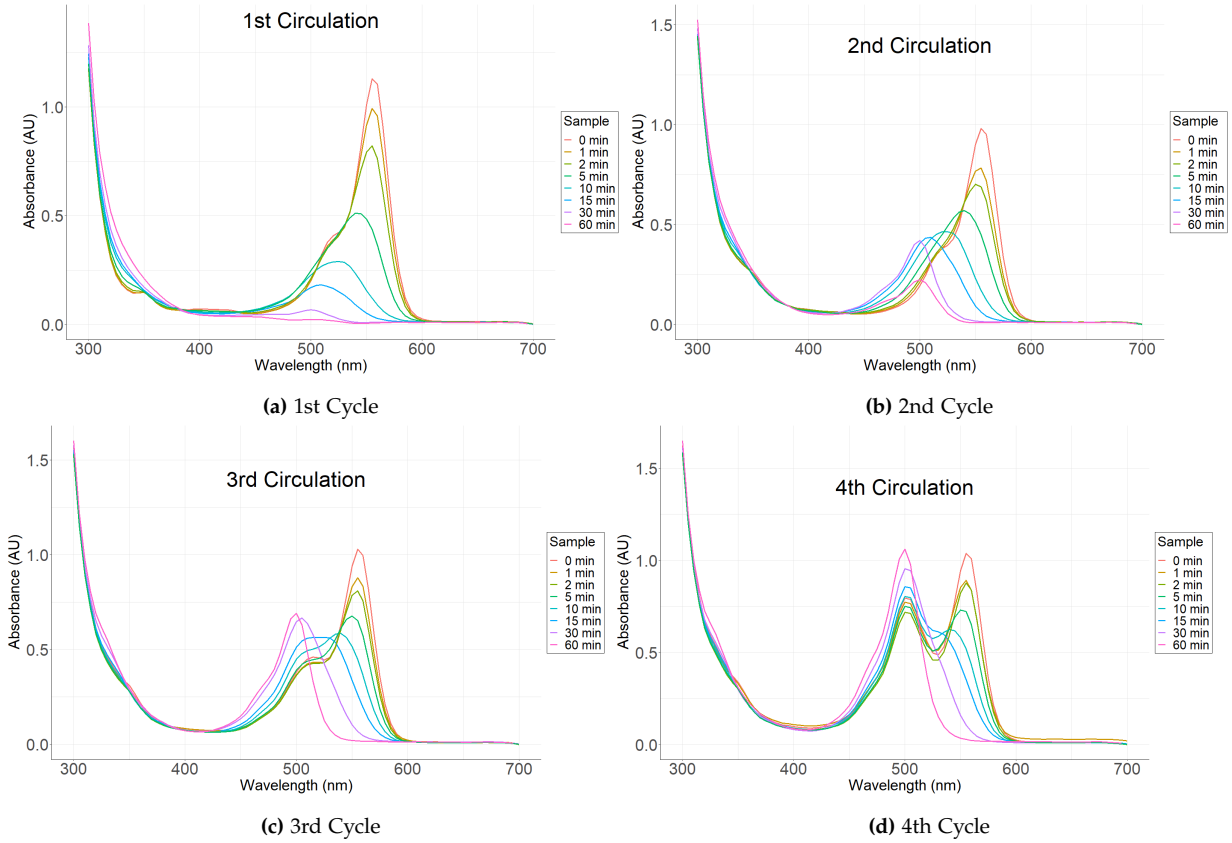


**(a)** 1st Cycle

**(b)** 2nd Cycle

**(c)** 3rd Cycle

**(d)** 4th Cycle

**Figure G.4:** Cycles for 5%Cu-doped $SrFeO_3$

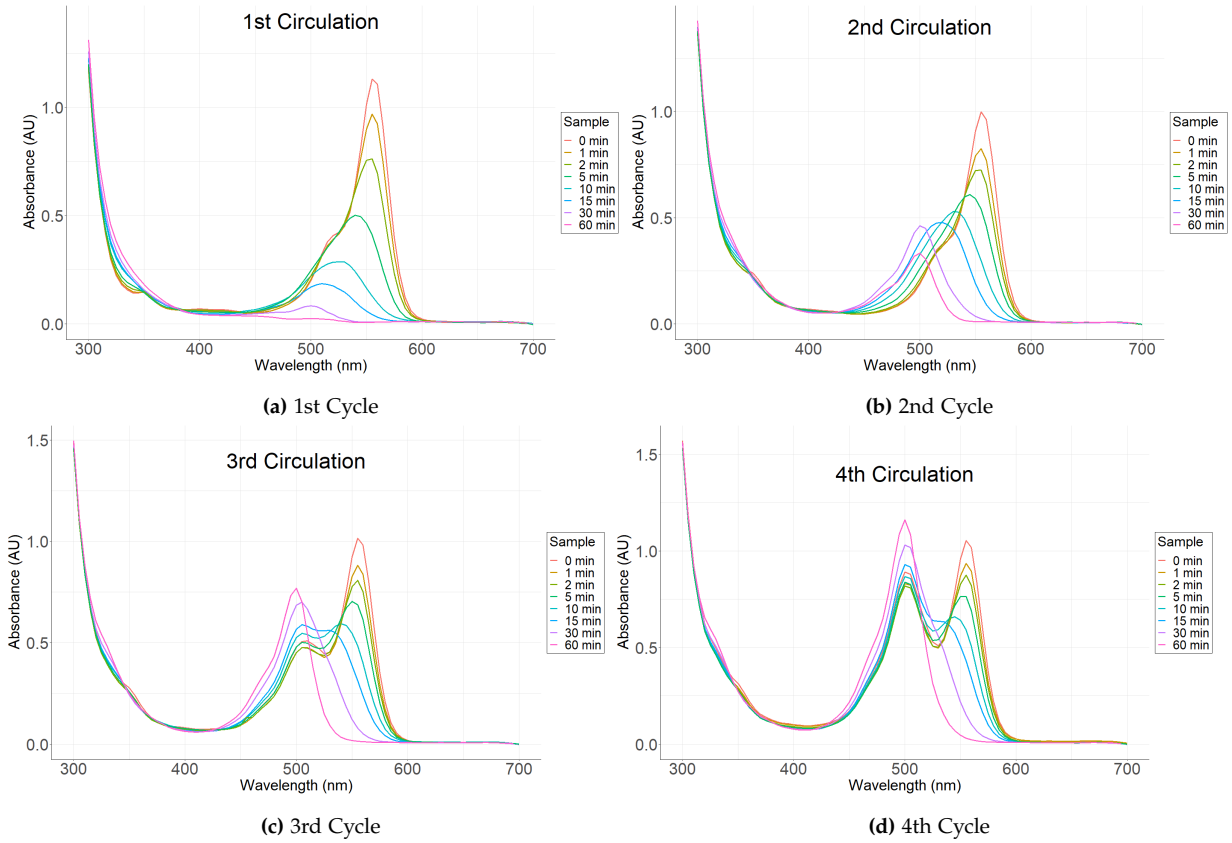


**(a)** 1st Cycle

**(b)** 2nd Cycle

**(c)** 3rd Cycle

**(d)** 4th Cycle

**Figure G.5:** Cycles for 10%Cu-doped $SrFeO_3$

# Appendix H
# Amount of leaching

| Perovskite | Temperature | %Sr-Leaching | %Fe-Leaching | %Cu-Leaching |
|---|---|---|---|---|
| 0% | 25 °C | 7.350 | 6.648 | -0.009 |
| | 35 °C | 9.923 | 8.839 | -0.007 |
| | 45 °C | 20.794 | 18.686 | -0.023 |
| | 55 °C | 27.276 | 24.017 | -0.009 |
| 1% | 25 °C | 6.3262 | 5.608 | 0.054 |
| | 35 °C | 12.036 | 11.286 | 0.112 |
| | 45 °C | 24.826 | 20.402 | 0.228 |
| | 55 °C | 33.486 | 25.772 | 0.321 |
| 2.5% | 25 °C | 6.978 | 6.768 | 0.195 |
| | 35 °C | 9.4740 | 9.335 | 0.281 |
| | 45 °C | 14.528 | 13.207 | 0.394 |
| | 55 °C | 36.269 | 29.113 | 0.889 |
| 5% | 25 °C | 6.011 | 5.867 | 0.408 |
| | 35 °C | 8.842 | 9.283 | 0.587 |
| | 45 °C | 12.267 | 12.035 | 0.771 |
| | 55 °C | 31.854 | 27.321 | 1.801 |
| 10% | 25 °C | 4.4563 | 4.708 | 1.198 |
| | 35 °C | 7.7813 | 8.159 | 1.864 |
| | 45 °C | 12.733 | 11.788 | 2.228 |
| | 55 °C | 33.732 | 29.852 | 4.352 |

**Table H.1:** Leaching % of different metals

| Perovskite | %SrLeach | %FeLeach | %CuLeach |
|---|---|---|---|
| 0% | 12.183 | 15.080 | 0.219 |
| 1% | 13.615 | 14.737 | 0.155 |
| 3% | 14.431 | 13.275 | 0.418 |
| 5% | 11.804 | 11.466 | 0.779 |
| 10% | 11.237 | 10.449 | 1.752 |

**Table H.2:** Leaching % of different metals after recycling 4 times

**Example of calculation of leaching %** The % of strontium in the perovskite is calculated to begin with:

$$\%Strontium_{perovskite} = \frac{M_{Sr}}{M_{SrFe_{0.95}Cu_{0.05}O_3}} \cdot 100\% = \frac{87.62g/mol}{191.85g/mol} \cdot 100\% = 45.67\% \quad \text{(H.1)}$$

The concentration can then be calculated of strontium:

$$Strontium_{perovskite} = \frac{m_{SrFe_{0.95}Cu_{0.05}O_3}}{V_{solution}} \cdot \%Strontium_{perovskite} = \frac{200mg}{200ml} \cdot 45.67\% = 0.4567g/L \quad \text{(H.2)}$$

Finally, the leaching% of strontium can be calculated:

$$\%SrLeached = \frac{LeachedSr}{[Sr_{perovskite}]} \cdot 100\% = \frac{145.49 \cdot 10^{-3}g/L}{0.4567g/L} \cdot 100\% = 31.86\% \quad \text{(H.3)}$$